Observations and Fine-Grid Simulations of a Convective Outbreak in Northeastern Spain: Importance of Diurnal Forcing and Convective Cold Pools

R. ROMERO

Cooperative Institute for Mesoscale Meteorological Studies, NOAA/National Severe Storms Laboratory, Norman, Oklahoma

C. A. DOSWELL III

NOAA/National Severe Storms Laboratory, Norman, Oklahoma

R. RIOSALIDO

Instituto Nacional de Meteorología, Madrid, Spain

(Manuscript received 11 May 2000, in final form 17 January 2001)

ABSTRACT

The life cycle and interactions of a series of convective systems that developed in northeastern Spain during the afternoon of 7 August 1996 are examined based on remote sensing products, surface observations, and numerical simulations. Most of the convection was organized in two mesoscale convective systems (MCSs) and a line of storms attached to the Pyrenees Mountains. One of these storms produced rainfalls in excess of 200 mm in 3 h and severe flash floods in the Biescas area. The end of the convection in the Biescas area occurred after merger of the storm with one of the MCSs that approached from the southwest. A high-resolution (4-km grid length) simulation of the event reproduces the observed timing and interactions of the convective systems, as well as the general rainfall pattern. The highly localized rainfall core at Biescas is well located, although the peak rainfall amount is underestimated. The success of the model at triggering the convection at the proper locations and time results from a reasonably accurate prediction of mesoscale features of the low-level flow pattern, such as a thermal mesolow in the Ebro valley, deformation zone, upslope wind systems, and the pushing of a cold front in the upper portion of the valley. After the onset of the initial convection, the role of the convectively induced cold pools and outflows for the propagation of the convective systems is shown to be very important. In particular, the MCS interacting with the Biescas convection was driven by strong mesoscale ascent established between the convectively induced outflows, the upvalley southeasterly winds sustained by the mesolow, and the downvalley northwesterly winds associated with the cold front. After the interaction, the convection in Biescas ceased because of the interruption of the southerly upslope flow caused by the convective cold pools. Finally, the explosive character of convection after noon and its initial focusing in uplands and slopes suggest that diurnal forcing could have played a decisive role. This idea is validated by means of simulations.

1. Introduction

Ordinary convective cells develop almost every afternoon during summer in northeastern Spain over the elevated terrain of the Pyrenees and Iberic System (Fig. 1). These storms are normally the result of the intense solar heating, which destabilizes the boundary layer, activates upslope and valley wind systems and the inflow of maritime air through sea-breeze circulations, and modulates an otherwise suppressive synoptic environment by means of a quasi-permanent thermal low over the dry Iberian plateau (Alonso et al. 1994). Except for the lightning threat, the summer convection is generally considered as beneficial for the region. However, when synoptic conditions are more supportive, as with cold air aloft, short-wave troughs moving over the region at upper levels, or when influenced by a passing cold front, convection can become more intense and extensive (as well as more organized and long lasting), and move well into the adjacent lowlands. Damaging hail events affecting the crops and fruit trees of the plains are not rare during the summer, and heavy rainfall is also a serious threat in areas of complex terrain. In particular, the evening of 7 August 1996 became infamous for the tragic consequences of a convective storm that developed in the Biescas zone (Huesca; see Fig. 1): more than 200 mm of rainfall between 1500 and 1800 UTC[1] caused a flash flood that severely damaged many infra-

Corresponding author address: Dr. Romualdo Romero, Dept. de Fisica, Universitat de les Illes Balears, 07071 Palma de Mallorca, Spain.
E-mail: dfsrrm8@ps.uib.es

[1] Local time in the region during summer corresponds to UTC+2 h.

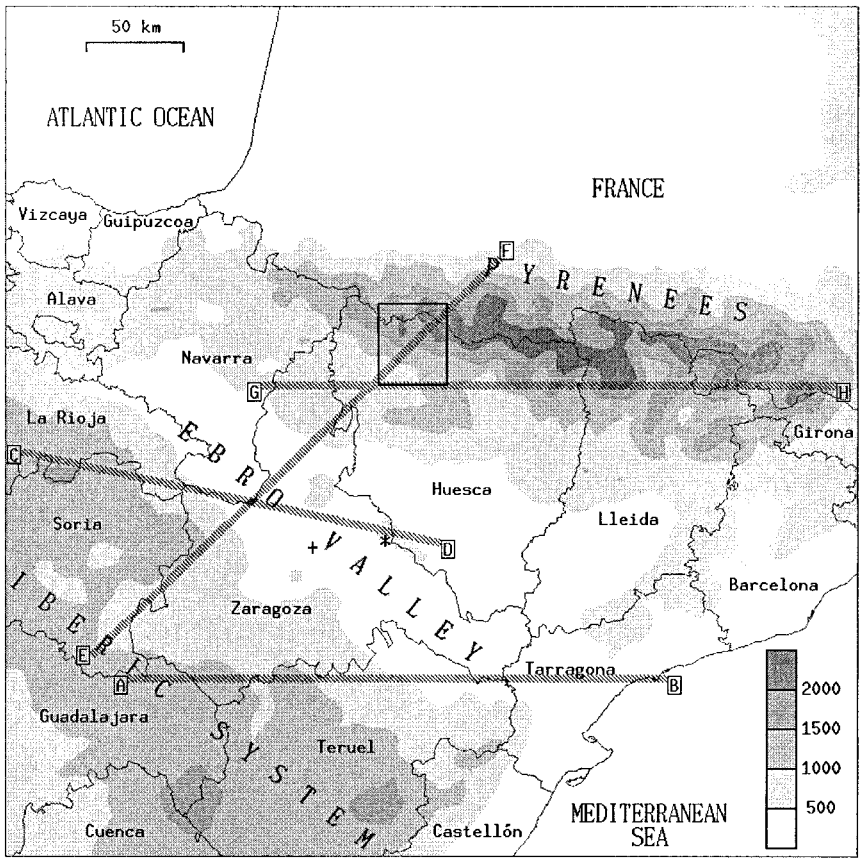

FIG. 1. Depiction of the northeastern region of Spain, with an indication of the main topographical units (uppercase) and the names of the administrative provinces (lowercase). The scale for the orography is expressed in m. The locations of the radar and radiosonde sites in Zaragoza are indicated by the asterisk and cross symbols, respectively. The positions of four vertical cross sections analyzed in the text are also indicated. The Biescas zone, where the flash floods occurred, is demarcated by the interior rectangle.

structures, utilities, and private properties, and more importantly, killed 86 people and injured other 93 in a camping site. The death toll was the highest for a flash flood event in Spain since 1973. Such a notorious event was obviously the result of a fatal combination of different components: notably, the hydrological component (important owing to the impermeability and steepness of the terrain), the ill-advised location of the camping area (on an alluvial fan), and the meteorological ingredients (particularly those responsible for the quasistationarity of the storm). This paper will focus mainly on the mesoscale meterological aspects of the event.

As illustrated in the next section, the storm at Biescas was only a small-scale[2] component of a widespread convective development that affected several provinces of northeastern Spain. Several convective systems coexisted in time. These systems generally exhibited differential movement speeds and directions [i.e., different combinations of the mean velocity of the constituting cells and the propagation velocity due to the formation of new cells; Chappell (1986)], and some of them even interacted with each other, as we will show in the next section. Therefore, the general evolution of the convection, dependent on both external and convectively generated mesoscale features of the flow, represents a challenging scientific and forecasting situation. A logical first issue is the response of a mesoscale numerical model faced with such a complex scenario. This is an issue worth exploring in order to anticipate the capability of high-resolution numerical prediction in the context of a future operational forecasting setting, where fine-grid mesoscale models are likely to be run. Mesoscale models applied to convective flash flood events under the current feasible conditions (grid lengths of 20–30 km and moderately sophisticated physical parameterizations) have already shown their potential for locating the general centers of heavy precipitation, especially in those areas where the orographic forcing is important (e.g., Romero et al. 2000). However, this by no means implies that with increased resolution and

[2] Radar reflectivities above 32 dBZ of the storm composed an area of about 400 km^2. The basin of the Arás Creek, responsible for the killing flood, measures only 20 km^2.

more complex or realistic physical parameterizations, more accurate spatial details, timing, and quantitative forecasts are guaranteed, especially when dealing with convection (Weisman et al. 1997). Some authors have suggested that it would be more desirable to dedicate the oncoming computational resources to different approaches, such as the ensemble forecasting, rather than devoting all resources to a continuing increase of model resolution and sophistication in hopes of obtaining the most accurate single forecast (Brooks and Doswell 1993; Brooks et al. 1995). On the other hand, some studies have shown explicitly the critical importance of a good representation in numerical models of mesoscale details of the low-level flow, such as outflow boundaries, for a good prediction of deep convective events, especially in those cases where the synoptic-scale forcing is not particularly strong or well defined (Stensrud and Fritsch 1994; Stensrud et al. 1999). These mesoscale features need to be incorporated properly in the model initial conditions if they have already developed at the beginning of the forecast period, or the model must be able to generate (or assimilate) them with enough spatial and temporal precision when they enter into play later during the simulation. In areas of complex terrain, mesoscale data assimilation and initialization may not always be necessary, since in such regions many of the mesoscale flow features result from the relatively deterministic interaction between synoptic-scale flow and orography (Colle and Mass 1996; Mass and Kuo 1998).

For the present case study, there are reasons to believe in the possibilities of a mesoscale model with certain optimism. This is because the orographic influences are particularly strong in the area (Fig. 1), and mesoscale models tend to resolve the orographic effects reasonably well provided they work at sufficient resolution. Although a detailed prediction of such a small phenomenon as the Biescas storm may not always be possible, a general depiction and physical interpretation of the mesoscale processes that evolved in the convective environment of 7 August 1996 seems possible and would be of value for the forecasters. This is the issue we wish to explore in this paper.

We begin with a summary of the event based on the observations in the next section. These observations are then complemented with the information of numerical simulations; section 3 describes the numerical model used and how the simulations were performed. While comparing the results against the observations for the purposes of model validation, model-generated information is used extensively in section 4 for the identification of the mesoscale processes that governed the initiation and evolution of the convection. Particular attention is paid to the effects of the diurnal forcing and convective cold pools. Finally, section 5 contains the conclusions of the study.

2. Observational aspects of the event

A technical report of this case based on upper-air and surface analyses, soundings, satellite imagery and radar scans was provided in Riosalido et al. (1998). In this section, we present part of that material, stressing the mesoscale details of the event that can be deduced from the observations and the spatial and temporal patterns of several fields that will be contrasted with the numerical simulations of section 4. Refer to Fig. 1 for locations mentioned in the text.

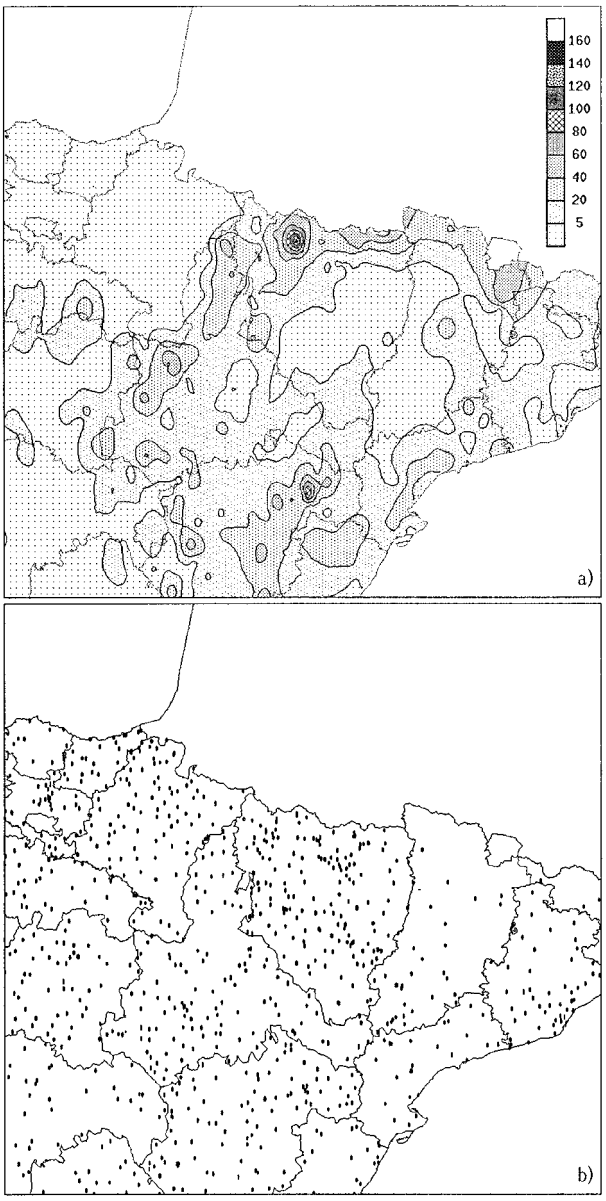

FIG. 2. (a) Analysis of the observed rainfall (mm) in northeastern Spain (Fig. 1) from 0700 UTC 7 Aug to 0700 UTC 8 Aug 1996. (b) Spatial distribution of the rain gauges used for the analysis.

An analysis of the observed rainfall between 0700 UTC 7 August and 0700 UTC 8 August (Fig. 2a) displays a peak value in the Biescas area. A rain gauge located very close to the camping site struck by the flash floods registered the maximum rainfall among all the available stations (Fig. 2b) during the 24-h period:

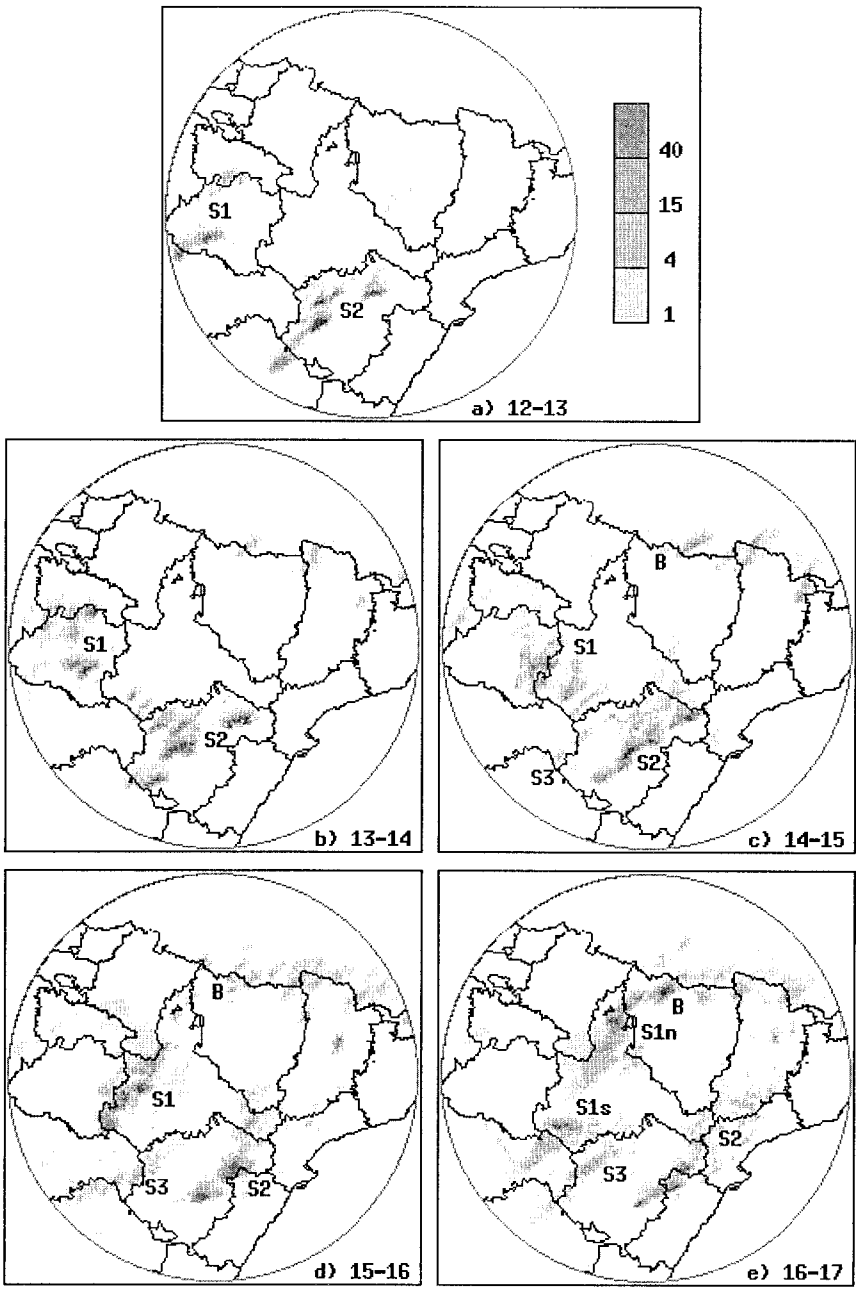

FIG. 3. Sequence of hourly rainfall estimates (mm) by the radar at Zaragoza from 1200 UTC 7 Aug to 2100 UTC 7 Aug 1996. Convective systems described in the text are indicated.

160 mm. By using radar-derived amounts corrected with local rainfall registers according to the spatially interpolated values of the logarithmic gauge–radar ratios (Koistinen and Puhakka 1984) during that period, Riosalido et al. (1998) estimated that the actual maximum likely exceeded 250 mm, with 225 mm accumulated between 1500 and 1800 UTC and 150 mm between 1600 and 1700 UTC. As reflected in Fig. 2a, rainfall greater than 5 mm was widespread in the northeastern provinces. The most important activity, however, was centered in northern Huesca and northern Lleida along the Pyrenees range, and between the Ebro valley and the Iberic System in Teruel, western Zaragoza, and the La Rioja–Soria boundary. Note also the corridor of substantial rainfall in the relatively low lands of northern Zaragoza and western Huesca that connects the aforementioned two precipitation areas. Other significant features are the precipitation centers next to the Mediterranean coast, a wide ring of low precipitation comprising the center and east of Zaragoza, east and south of

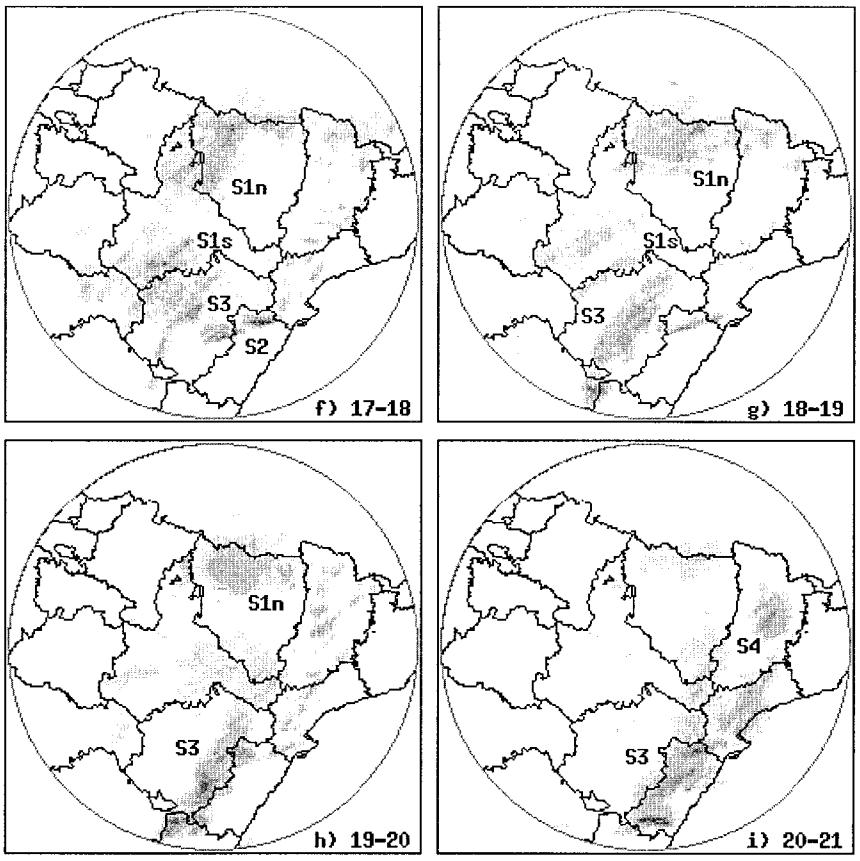

FIG. 3. (*Continued*)

Huesca and majority of Lleida, and the limited rainfalls observed within the upper portion of the Ebro valley in Navarra. The spatial distribution of rain gauges (Fig. 2b) used for the rainfall analysis reveals some gaps in Lleida and Girona that may have caused underestimation of rainfall in the eastern Pyrenees. Other gaps in the rest of provinces also might have influenced the analysis adversely, especially the intensity, shape, and number of maxima, but the density and homogeneity of stations seem adequate to characterize the main aspects of the rainfall field.

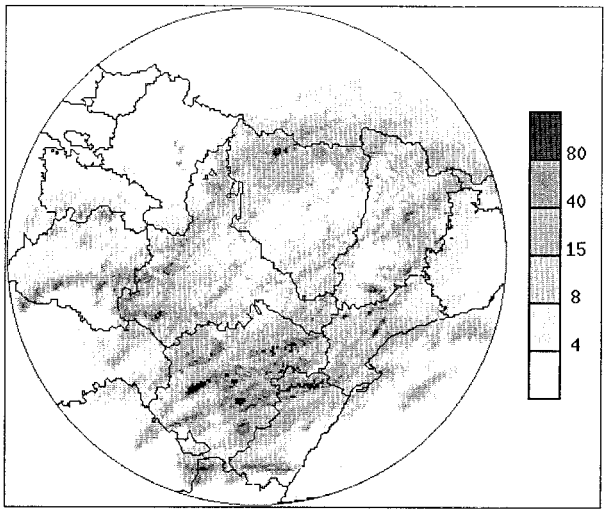

FIG. 4. Total estimated rainfall (mm) by the radar at Zaragoza from 0700 UTC 7 Aug to 0700 UTC 8 Aug 1996.

Only a very few of the stations are automatic and able to provide higher temporal resolution than the 0700–0700 UTC 24-h totals. Therefore, a detailed temporal history of the convective episode cannot be derived from the rain gauge network. For that purpose, we have considered the information provided by the Zaragoza radar,[3] located approximately at the center of the region (Fig. 1). The episode began early in the afternoon, at about 1200 UTC (Fig. 3), suggesting that diurnal heating could be an important factor. Earlier convective developments occurred in response to the approaching midtropospheric trough, but these developments, aligned in SW–NE bands, had very limited vertical and horizontal extent and moved northeastward very quickly.

The convection started on the slopes and peaks of the

[3] The operational Z–R relation for convective precipitation $Z = 800R^{1.6}$ has been used to estimate rainfall amounts. Reflectivity scans are made every 10 min.

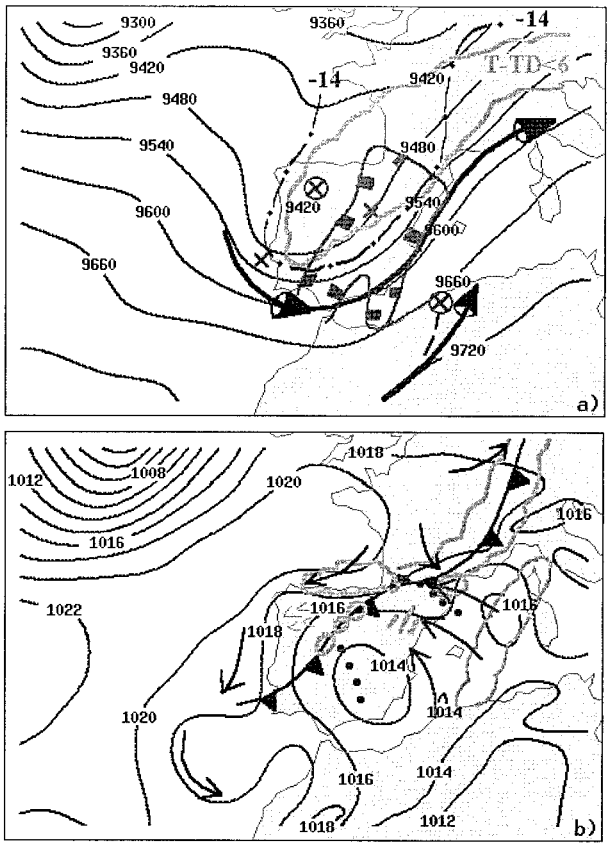

FIG. 5. Synoptic composite charts at 1200 UTC 7 Aug 1996 (from Riosalido et al. 1998). (a) For mid- and upper-tropospheric levels, showing geopotential height at 300 hPa, jet streaks (arrows), the area with upward quasigeostrophic forcing at 500 hPa (contour with squares), curvature and shear vorticity maxima at 500 hPa (crosses with and without circle, respectively), area with dewpoint depressions at 500 hPa less than 6° (scalloped contour), and the −14°C isotherm at 500 hPa (dotted–dashed line). (b) For low-tropospheric levels, showing sea level pressure, the surface cold front, thermal ridge axis at 850 hPa (dotted), cold and warm air advection at 850 hPa (arrows northwest and east of the front, respectively), and significant cloudy areas.

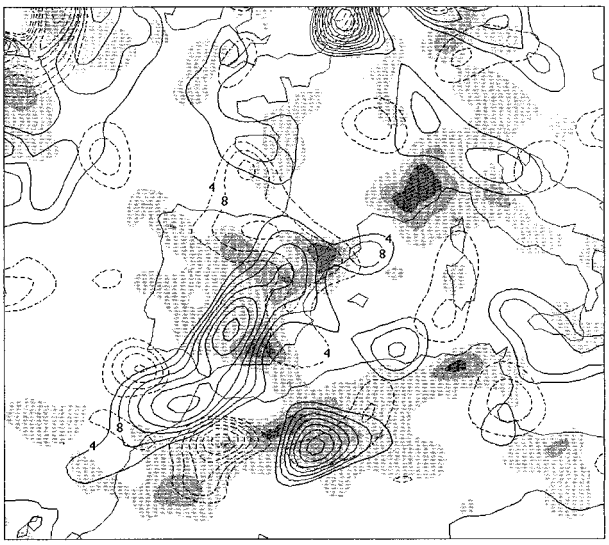

FIG. 6. Upward quasigeostrophic forcing at 500 hPa (continuous line) and at 850 hPa (dashed line) and values of water vapor flux convergence in the layer 1000–850-hPa greater than 0.05, 0.25, and 0.45 g m^{-2} s^{-1} (shaded) on 1200 UTC 7 Aug 1996, derived from NCEP grid analyses. The quasigeostrophic forcing is calculated following the *Q* vector formulation (Hoskins and Pedder 1980) and its contour interval is 4×10^{-18} m kg^{-1} s^{-1} starting at 4×10^{-18} m kg^{-1} s^{-1}.

Pyrenees and Iberic System and was initially confined around these zones (Figs. 3a and 3b). An analysis of cloud-top temperatures derived from infrared Meteosat imagery (not shown) reveals that the convective cells in Soria and La Rioja were part of the same mesoscale convective system (S1), whereas the convection that developed over Teruel was organized in another mesoscale convective system (MCS) (S2). During the first hours, both MCSs progressed eastward from their initial locations over the mountains (Figs. 3a–d). Intermittently, the anvil shields of these systems appeared to be connected. At about 1500 UTC, the convective development that was to affect Biescas was already visible at the western extreme of the chain of convective cells attached to the Pyrenees (B in Fig. 3c). Unlike the bigger systems S1 and S2, B remained basically stationary during the subsequent hours, gaining in intensity and areal extent and extending downslope from its genesis area on the mountain peaks of the Spain–France boundary (see orography in Fig. 1). At 1600 UTC, both S1 and S2 had evolved to a structure elongated in the SW–NE direction, and the first cells of another convective system (S3) that would grow explosively later on the day were evident (Fig. 3d).

From that time (Figs. 3d–i), the evolution of the convective systems changed significantly, probably as a consequence of the complex disruption of the flow by the convection itself, making this case both attractive and difficult. While system S2 continued its eastward movement until its dissipation at about 1900 UTC, system S1 started to exhibit a northeastward movement (S1n) at the same time that other active cells developed on the southwestern part of the convective band over southern Zaragoza (S1s). After 1700 UTC, system S1n merged with the convective storms of the Pyrenees, losing its elongated structure with time and undergoing a gradual dissipation. In particular, precipitation rates in the Biescas zone decayed rapidly after the interaction of storm B with system S1n at 1800 UTC. Meanwhile, system S1s also decayed, whereas the nearby system S3 grew and intensified very rapidly, dominating the situation as a squall line by 2100 UTC (Fig. 3i).

The total estimated rainfall by the radar of Zaragoza (Fig. 4) can be compared with the analysis derived from the rain gauges (Fig. 2). There is a general agreement between the spatial patterns of both products, but the radar-derived quantitative amounts are generally greater, especially in Teruel and western Zaragoza. As noted by

Riosalido et al. (1998), it is possible that the presence of hail in some of the thunderstorms of Teruel had resulted in overestimation of rainfall in that area.

Riosalido et al. (1998) summarized the synoptic environment in which the convective outbreak occurred by means of composite charts (Fig. 5). The synoptic situation at midtropospheric levels (Fig. 5a) was characterized by the advance of a trough and cold front. This favored an increase of potential instability and a general pattern of upward quasigeostrophic forcing over the eastern half of the Iberian Peninsula (Fig. 6). The approach of an embedded vorticity maximum into northeastern Spain along the downstream section of the main trough likely enhanced large-scale ascent. By 1200 UTC, the axis of the southwesterly upper-level jet had passed the eastern coast of Spain (Fig. 5a). Over the region of interest, the decrease of the upper-level winds corresponded with slower storm motions and smaller anvils in the convection that developed after noon than in the early morning convection.

The synoptic situation at low levels (Fig. 5b) was dominated by a low centered over southeastern Spain and a cold front extending between central Europe and Portugal through northern Spain. The cold front affected the upper portion of the Ebro valley during the day but its progression was very slow, perhaps owing to the blocking action of the Pyrenees. Diagnostic calculations reveal a pattern of upward quasigeostrophic dynamic forcing at 850 hPa overlapping with the upward forcing field at 500 hPa over northeastern Spain, as well as notable low-level water vapor flux convergence over the same area, established between the cold front and the low-induced maritime, warm southeasterly flow (Fig. 6).

The evolution of the synoptic pattern during 7 August is reflected in the observed soundings at the Zaragoza station (indicated by a cross in Fig. 1). At 0000 UTC (Fig. 7a) the precipitable water is 33 mm, the lifted index (LI) is +1, the *K* index (*K*) is 35, the total totals index (TT) is 51, the convective available potential energy (CAPE) for the surface parcel is 31 J kg^{-1}, and its convective inhibition (CIN) is 383 J kg^{-1}. The sounding at 1200 UTC (Fig. 7b) reflects a significant steepening of the middle- and upper-tropospheric lapse rates and a decrease of the winds around 500 hPa, associated with the approach of the synoptic-scale trough. Despite warm advection in the lower troposphere, the occurrence during the morning of cool northwesterly flow channelled along the Ebro valley produced a significant cooling of the atmosphere below that level and a marked thermal inversion between 850 and 800 hPa (Fig. 7b). At 1200 UTC, the precipitable water increased to 37 mm and the stability indices indicate a higher probability of convection (LI, −2; K, 35; TT, 55; and CAPE, 945 J kg^{-1}). However, convective inhibition was 165 J kg^{-1} as a consequence of the stable layer next to the ground. Therefore, the available sounding suggests that significant lifting was necessary for the surface parcels to reach their level of free convection, at least within the Ebro valley. The representativeness of the Zaragoza sounding for the mountainous areas is more questionable, especially for describing the near-ground conditions.

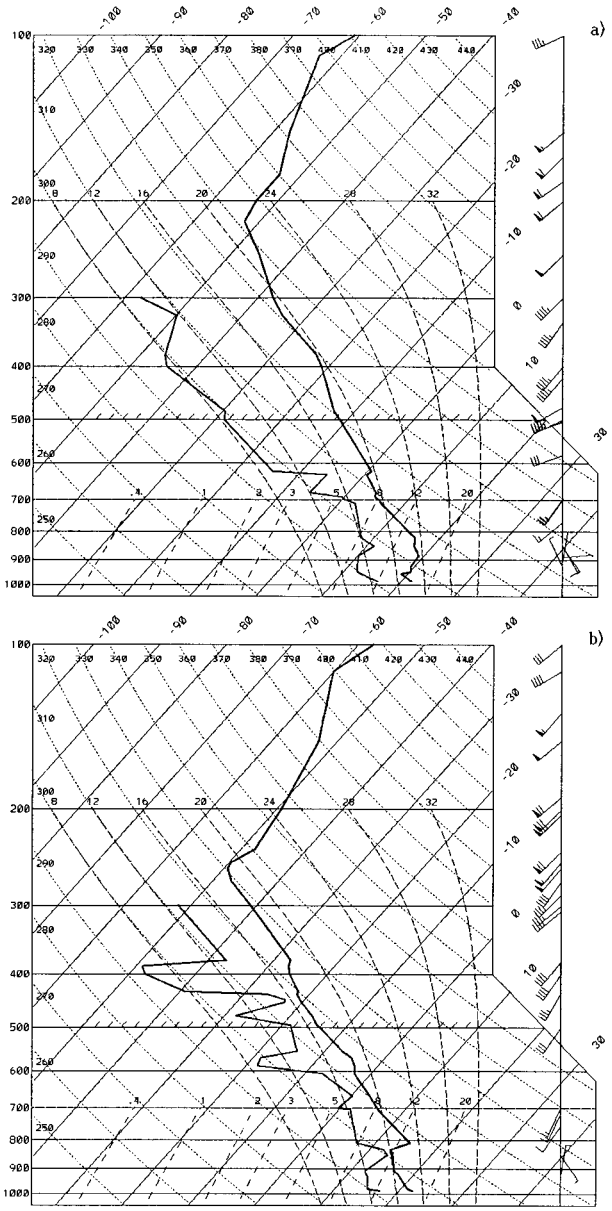

FIG. 7. Radiosounding at Zaragoza on 7 Aug 1996 at (a) 0000 and (b) 1200 UTC. Full wind barb is 5 m s^{-1}.

In addition to a favorable synoptic-scale context, mesoscale lifting mechanisms are normally required to initiate and sustain deep convection (Doswell 1987). Mesoscale ingredients for this event appear to be related to the organization of the low-level flow and to the orography. The surface composite charts shown in Fig. 8 summarize the main aspects of the low-level flow observed during the initial stage of the episode. The

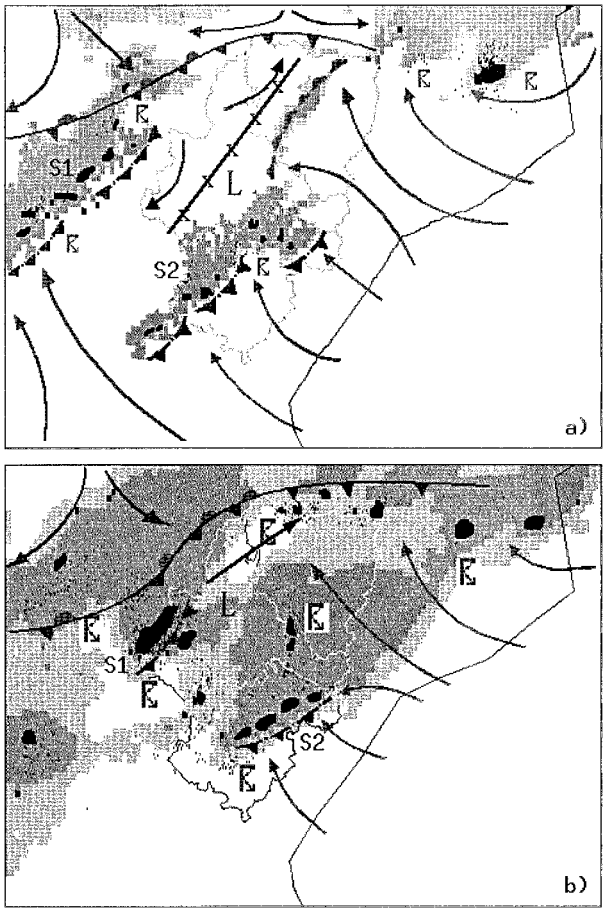

FIG. 8. Surface mesoscale composite charts for northeastern Spain on 7 Aug 1996 at (a) 1200 and (b) 1500 UTC (from Riosalido et al. 1998). The charts show streamlines, deformation zone in (a) represented by the dilatation axis, cold cloud tops as indicated by infrared channel of Meteosat (light and dark shaded), intense radar echoes (black areas), lightning activity (conventional symbol and black dots), front, outflow boundaries, warm boundary in (a), and the mesolow developed in the central and upper portions of the Ebro valley (L). The provinces of Huesca, Zaragoza, and Teruel are included as reference.

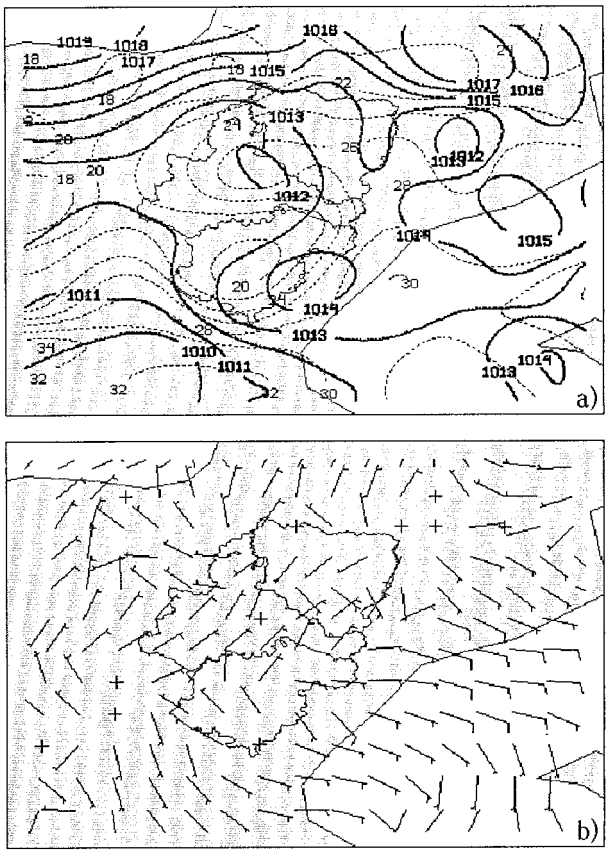

FIG. 9. Regional surface objective analyses on 7 Aug 1996 at 1500 UTC (from Riosalido et al. 1998). (a) Sea level pressure (continuous line, in hPa) and surface temperature (dashed line, in °C). (b) Surface wind (half and full wind barbs represent 5 and 10 kt, respectively). The provinces of Zaragoza, Huesca, and Teruel are included as reference.

upper part of the Ebro valley was affected by cool northwesterly winds associated with the front, whereas the general flow was from the southeast, directly from the Mediterranean waters. The streamlines were deflected toward the slopes of the Pyrenees and Iberic System, probably as a result of the diurnal heating. A SW–NE-oriented deformation zone was positioned across western Zaragoza and western Huesca, with sustained south-southwesterly upslope winds in the Biescas area. An intensifying mesolow in the Ebro valley during the afternoon of thermal origin (as suggested by its warm core), as well as the slow downvalley progression of the cold front, combined to enhance the inflow and convergence toward northern Zaragoza and western Huesca. Presumably, the convectively generated cold pools and outflow boundaries also conditioned the subsequent evolution of the convective systems in a complex way.

Unfortunately, the current observations density in the area does not offer enough resolution to sample adequately small-scale features of the flow such as the convectively induced perturbations. The finest possible detail is contained in the regional surface objective analyses routinely used at the Spanish Instituto Nacional de Meteorología. These analyses (see Figs. 9 and 10 for 1500 and 1800 UTC), used to draw the previous composites, are constructed from the surface synoptic observations (only four or five per province at most) using as a first guess the output of the 0.2° resolution operational model. Despite the smoothness and limitations of the analyses, some embedded features of the flow field appear to be plausible and interpretable. These features include the cold pool and relative high pressures around Teruel, which would be associated with the convection evolving over that area; the relatively cool temperatures also observed west of Zaragoza where the convective system S1 occurred; and the veering of the winds to northwesterlies in northern Zaragoza and western Huesca at 18 UTC, consistent with the progression of the cold front and the outflow winds developed by

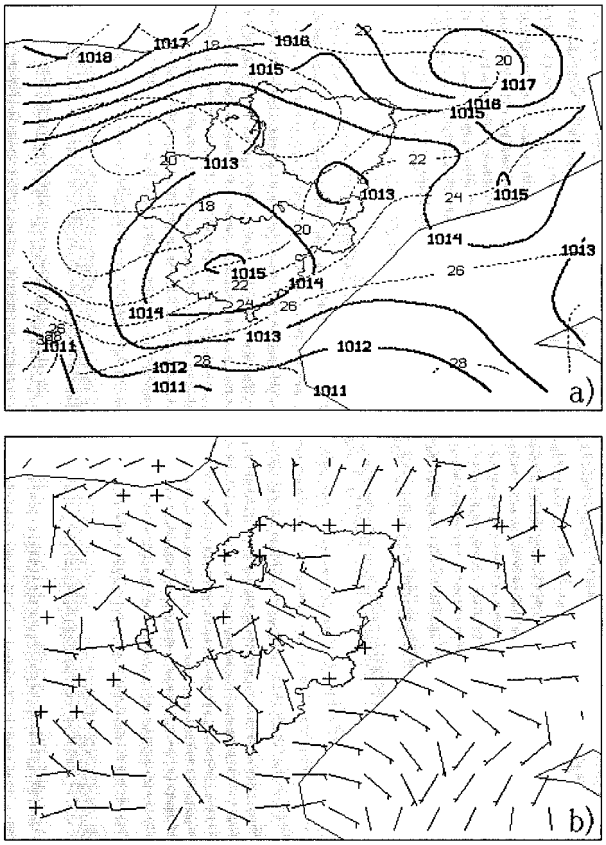

FIG. 10. As in Fig. 9 but on 7 Aug 1996 at 1800 UTC.

S1n. Other significant features seen in Figs. 9 and 10 are the warm core mesolow of the Ebro valley, mentioned previously, and the blocking high pressure area north of the Pyrenees.

3. Numerical model and simulation characteristics

For the purpose of better identifying and evaluating the mesoscale processes that governed the particular mode of initiation and evolution of the convection, a simulation of the event was designed using the nonhydrostatic version of the Pennsylvania State University–National Center for Atmospheric Research (NCAR) fifth-generation Mesoscale Model (Dudhia 1993; Grell et al. 1995).

The model is formulated using the terrain-following σ coordinate system, with enhanced vertical resolution in the lower troposphere to represent adequately the boundary layer processes. A convenient feature of the model is its multiple-nest capability, with two-way interaction between sucessive nesting levels that allows realistic terrain features (Zhang et al. 1986). The present study requires a sufficiently high grid resolution for an adequate representation of the convective systems and proper incorporation of the terrain features. Therefore, three sucessively nested domains with horizontal grid

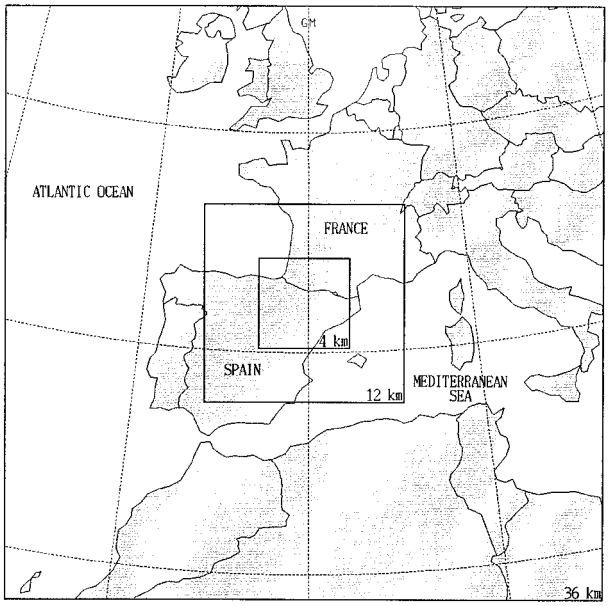

FIG. 11. Geographical location of the domains used for the simulations.

spacings of 36, 12, and 4 km were considered (Fig. 11). The three domains are centered at a same point in Huesca (42.25°N, 0.25°W) under a Lambert conformal map projection and comprise the same 31 σ vertical levels. In the horizontal, they contain 82 $\times$ 82, 82 $\times$ 82, and 112 $\times$ 112 grid points, respectively. The 4-km grid domain and its orography, constructed from global 30″ elevation data provided by the U.S. Geological Survey (USGS), are those shown in Fig. 1. Initial and boundary conditions for the 36-km grid are constructed from a

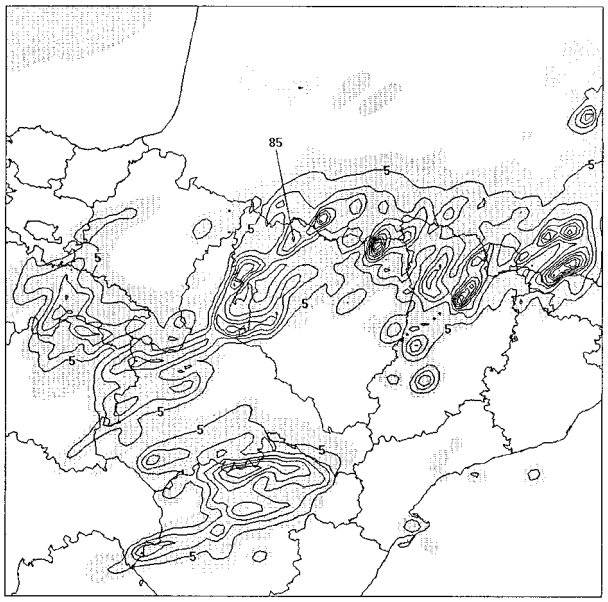

FIG. 12. Forecast total precipitation. Contour interval is as in Fig. 2a, with the shaded areas indicating rainfall in excess of 1 mm.

first guess produced by horizontal interpolation of the global analyses from the National Centers for Environmental Prediction (NCEP), which then is modified using surface and upper-air observations with a successive-correction objective analysis technique (Benjamin and Seaman 1985). The resulting fields are interpolated to the model σ levels, and initial imbalances of the interpolated fields are reduced by removing the vertical integral of the horizontal divergence in each grid point (Washington and Baumhefner 1975). The initialization process is completed with interpolation of the coarse grid fields to the 12- and 4-km resolution grids. The tendencies of the fields along the model coarse domain boundaries are applied using a Newtonian relaxation approach (Grell et al. 1995).

The model incorporates several options for the physical parameterizations. In the present experiments, the parameterization scheme used to represent the planetary boundary layer physics is a modified version of the Blackadar (1979) scheme (Zhang and Anthes 1982; Zhang and Fritsch 1986). Surface temperature over land is calculated using a force–restore slab model (Blackadar 1979; Zhang and Anthes 1982), and over sea remained constant during the simulation. A discrimination of up to 14 different surface types in the fine-grid domain is possible, based on global 30″ vegetation data from the USGS. Surface fluxes, as well as atmospheric temperature tendencies caused by longwave and shortwave radiation components, are calculated taking into account the cloud cover (Benjamin 1983).

Resolved-scale microphysics and moist convection parameterization schemes are selected in accordance with the different grid resolutions. For the coarse grid, explicit microphysics is represented with predictive equations for cloud water and rainwater below the freezing level, and cloud ice and snow above the freezing level (Dudhia 1989), including the effects of hydrostatic water loading, condensation, evaporation, melting, freezing, deposition, and sublimation (Zhang 1989), but not supercooled liquid water. Parameterized convection is formulated using the Kain–Fritsch scheme (Kain and Fritsch 1990). For the 12- and 4-km resolution grids, a more complex bulk mixed-phase microphysical model based on the work by Lin et al. (1983) is used (Tao and Simpson 1993). It includes predictive equations for cloud water, rain, snow, cloud ice, and graupel (see Tao and Simpson 1993 for details). For the 12-km resolution grid, the cumulus parameterization scheme of Grell (1993) is used, which, as that work shows, allows the balance between the explicit and the implicit representation of convection required for a correct modelling of midlatitude MCSs at these resolutions (Zhang et al. 1989). For the finest grid, no cumulus parameterization is included, owing to its short horizontal grid length.

NCEP global analysis are available at 0000 and 1200 UTC. As described in last section, the first convective systems developed at about 1200 UTC on 7 August 1996. The simulation presented extends 24 h, starting at 0000 UTC on that day. It would seem that a simulation starting at 1200 UTC could suffice, but such a simulation (not included) was shown to be of poor quality. This is not unexpected, since the results are probably affected by model spinup processes and, more importantly, relevant aspects of the flow associated with the solar heating (discussed in next section) cannot be properly developed by a simulation that starts 7 h after sunrise.

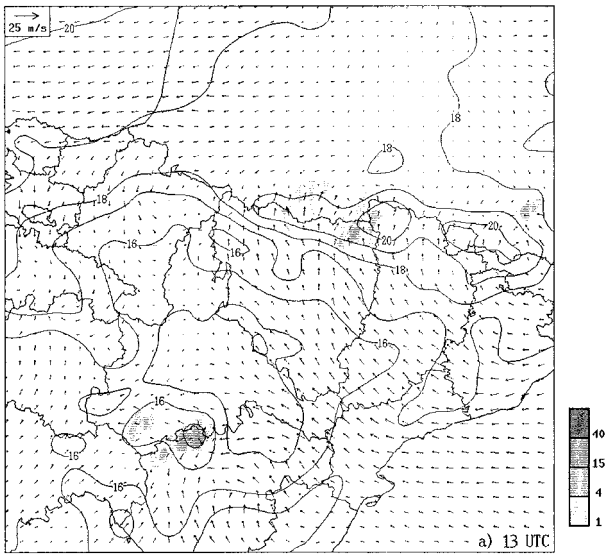

FIG. 13. Time sequence of model-predicted hourly rainfall [in mm, according to the grayscale shown in (a)], sea level pressure (in hPa without the leading 10), and wind field at 925 hPa [vectors shown every three grid points; a reference vector is included in (a)], for the period 1300 UTC 7 Aug–2100 UTC 7 Aug 1996. Hourly rainfall refers to the 1-h period ending at each time shown, thus in close correspondence with Fig. 3. Highs, lows, convective systems, outflow boundaries, and convergence lines (dashed) mentioned in the text are indicated.

4. Results and discussion

In terms of the forecast rainfall field (Fig. 12), the primary simulation appears to be sufficiently validated. The observed general structure of this field (Fig. 2a) is basically well captured by the simulation, that is, the two general bands of substantial precipitation along the Pyrenees and northeast-facing slopes of the Iberic System, and the connecting corridor along northern Zaragoza and western Huesca. Also, the low precipitation areas of Zaragoza, Huesca, Lleida, and Navarra are reasonably well delimited. The major deficiencies occur along the Mediterranean coastal provinces, where the simulation indicates either no precipitation or too little precipitation. Although it is true that some fraction of the analyzed rainfall for those provinces in Fig. 2a was observed later than 0000 UTC 8 August (simulation end time), it also will be seen how the model has some difficulties in maintaining the activity of the mature convective systems that enter those provinces from the west.

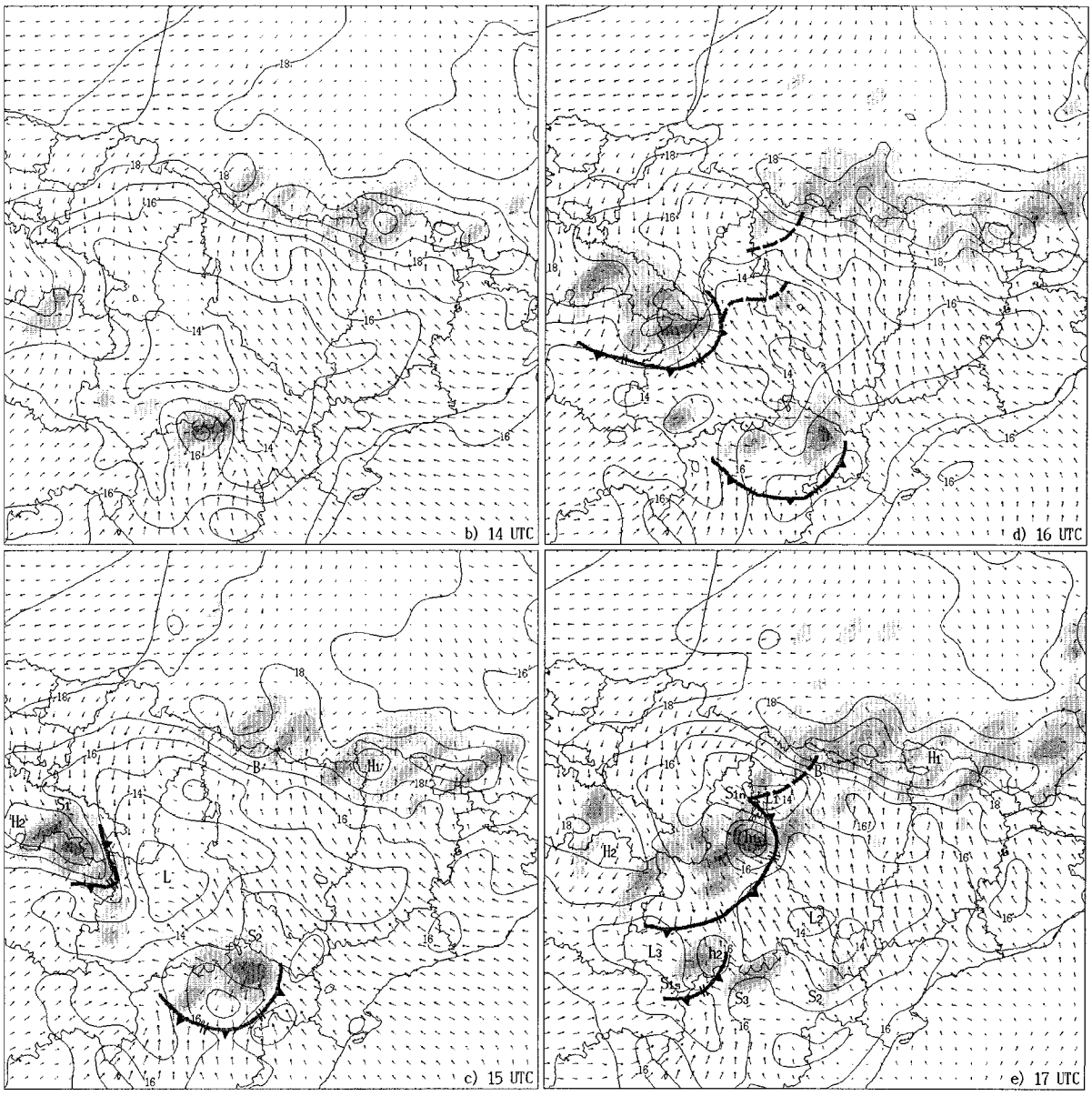

FIG. 13. (*Continued*)

On the other hand, the precipitation maxima are generally more intense in the simulation than in the observations or even the radar estimates (Fig. 4). Many of the forecast maxima are somewhat misplaced, less than 20–30 km in general. Interestingly, the model locates very accurately the precipitation center at Biescas, with a moderate peak amount of 85 mm (Fig. 12) and a spatial average over the interior region shown in Fig. 1 of 31 mm. The same average computed from the analysis of the observed rainfall (Fig. 2a) yields 45 mm. Other local maxima simulated in other zones of the Pyrenees range are greater than the Biescas maximum and, in fact, appear to be too stong compared with the observations. It is clear that the capability of the mesoscale model to capture the exact position and relative importance of local precipitation centers is very limited. Even so, the forecast shown in Fig. 12 could be considered useful guidance, suggesting the potential for flash floods in the southern basins of the Pyrenees on that day.

The capability of the model to capture the timing of the event is certainly remarkable, as can be verified by comparing the observed sequence of hourly rainfall (Fig. 3) with the same field computed from the simulation (shaded areas in Fig. 13). This result offers some confidence that the mesoscale processes identified and discussed in the following sections actually evolved more or less in the way and strength indicated by the simulation.

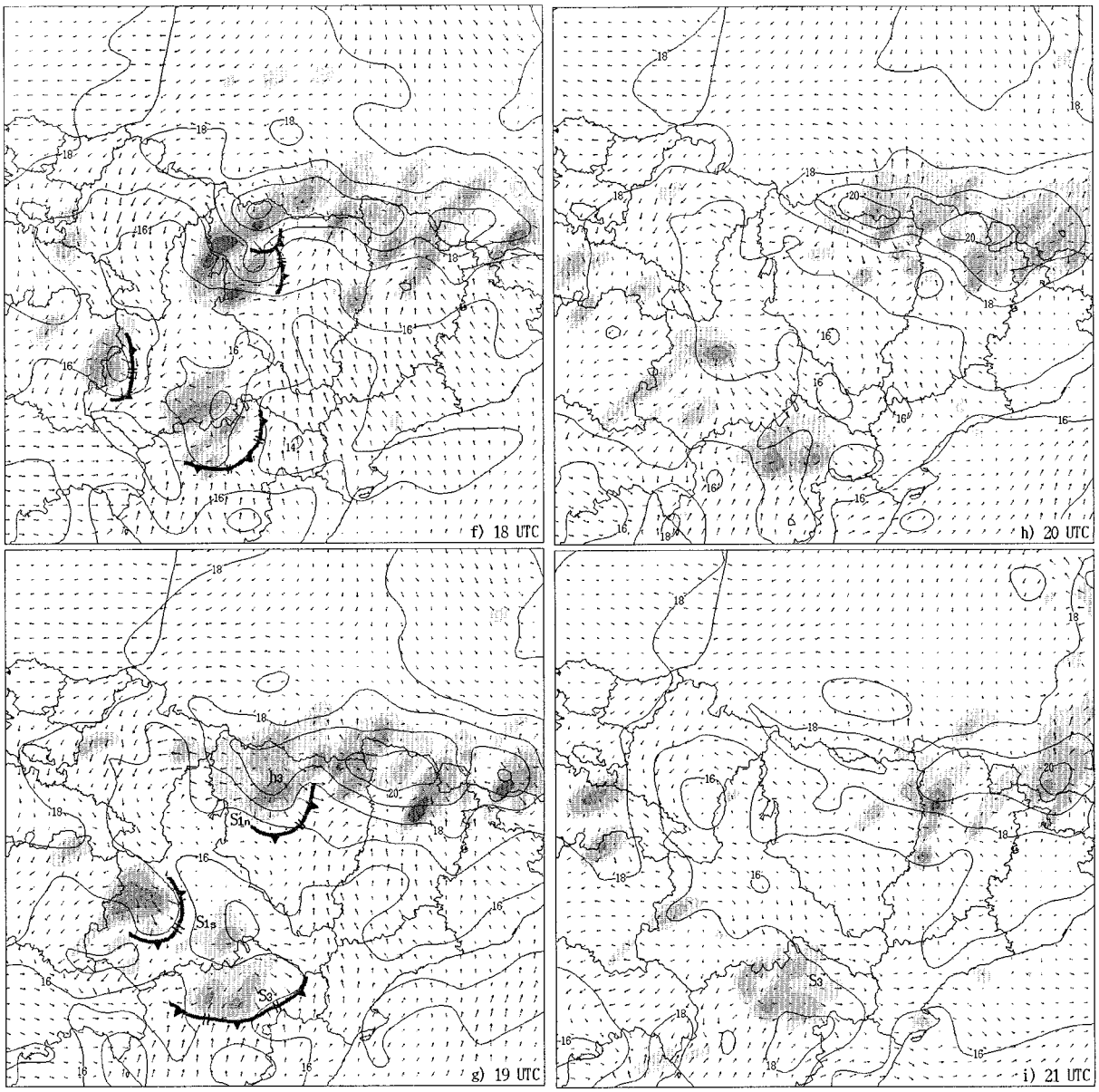

FIG. 13. (*Continued*)

a. Evolution of the convection and governing mesoscale processes

Figure 13 summarizes the evolution of the simulated convective event from its beginning at noon until 2100 UTC, when most of the inland convection started to dissipate. The initial stage of the episode (Figs. 13a–c) reflects the simultaneous triggering of the convection in northern Teruel (convective system S2), La Rioja and Soria (system S1), and along the Pyrenees Mountain chain, in close agreement with the observations (Fig. 3). However, part of the convection of S2 that was observed in its southern extreme, over central Teruel, is not present in the simulation.

The triggering of the initial convection is certainly rooted in the appreciable lifting provided by the slopes of the Pyrenees and Iberic System. General upslope wind flows are simulated, as displayed in Fig. 13a. In particular, the flow entering the Ebro valley from the Mediterranean is deflected toward the mountains of Teruel, providing an east-northeasterly wind component, and toward the southern slopes of the Pyrenees, there providing a substantial southerly component. In the upper portion of the Ebro valley, the flow is directed toward the mountains of La Rioja and Soria. This flow pattern is thus very similar to that displayed in the surface composite charts (Fig. 8). Further, the deformation zone observed across western Zaragoza and western Huesca is very well captured by the simulation, being

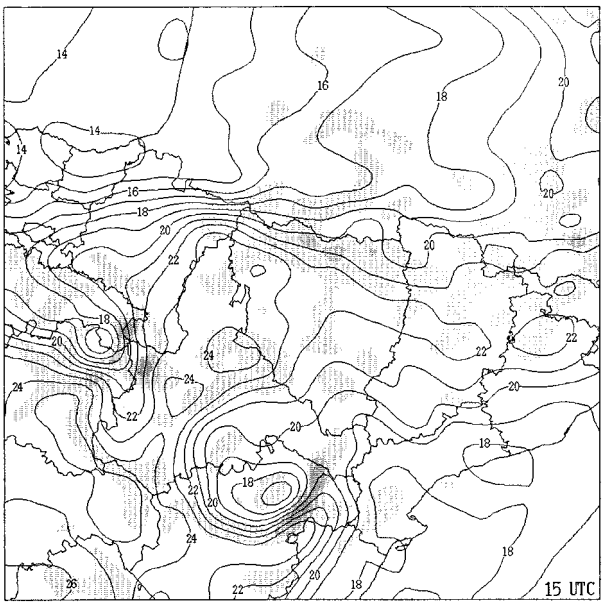

FIG. 14. Model-predicted temperature field at 925 hPa (°C, continuous line) and areas of upward motion at 850 hPa exceeding 0.1, 0.5, and 1 m s^{-1} (light, medium, and dark shaded, respectively) for 1500 UTC 7 Aug 1996.

most clear at 1500 UTC (Fig. 13c). Another important feature that conditioned the low-level flow, the mesolow in the Ebro valley (L), is properly developed in the simulation. The mesolow, already clear at 1100 UTC (time not shown), deepens appreciably between 1200 and 1500 UTC, the period in which the ground temperatures on the dry lowlands of the Ebro valley are the highest. The deepening of the mesolow is noted in the intensification of the southeasterly and northwesterly winds toward the center of Zaragoza, where the mesolow is located. Other remarkable and persistent features of the sea level pressure field are the blocking high pressure areas found along the north-facing flanks of the Pyrenees (H1) and Iberic System (H2), against which the cold front is trapped (Fig. 8b).

While growing in size, during the first hours the simulated convective systems S1 and S2 move from their genesis areas to the east-southeast in the same way as observed (Figs. 3a–c), approximately following the topography of the Iberic System. This movement appears to be regulated by the generation of new cells that are due to lifting provided by the upslope winds along the range, probably enhanced by the action of the outflows from previous convective areas. In fact, outflows due to S1 and S2 are already evident at 1400 UTC (Fig. 13b), becoming still more so at 1500 UTC (Fig. 13c). At that time, the outflows are quite spread out and their boundaries define areas of enhanced convergence in eastern Teruel and western Zaragoza, quite in agreement with the position indicated by the observations (Figs. 8b and 9). Obviously, the outflow boundaries are preferential areas for ascent and development of new convection, and this is reflected in a farther eastward progression of S1 and S2 (Fig. 13d).

On the other hand, the generation of the outflows is associated with an increase of the sea level pressure around the areas of precipitation (Figs. 13a–d). This fact is consistent, under hydrostatic considerations, with an origin in the evaporatively cooled downdraft air from the precipitating clouds. Indeed, the development of cold pools by both S1 and S2 is nicely illustrated in Fig. 14, which shows the 925-hPa temperature field at 1500 UTC, which is consistent with the regional objective analysis of Fig. 9a. Quite extensive negative temperature perturbations are simulated in northern Soria and western Zaragoza, and northern Teruel and southern Zaragoza, respectively. Other significant features of the temperature field are a strong gradient directed across the Pyrenees, Navarra, and Alava as a consequence of the cold front, and a temperature maximum in central Zaragoza where the mesolow is located, suggesting thus a thermal origin of the low. As expected, narrow arc-shaped zones of intense upward motion at low levels are found along the leading edges of the spreading cold pools (Fig. 14), especially where the outflow boundaries were identified. Significant upward motion is also predicted in central Zaragoza, and along the southern slopes of the Pyrenees from eastern Navarra to western Girona.

Starting at 1500 UTC, the low-level flow pattern becomes very complex, as a consequence of the disruption produced by the convectively generated cold pools and outflows interacting with the complex terrain. These features are probably influencing the evolution and propagation of convection very strongly (this aspect will be the specific topic of section 4d). The different movements of the convective systems S1 and S2 between 1500 and 1800 UTC noted in the radar images (Figs. 3d–f) are also indicated by the simulation (Figs. 13d–f). On one hand, system S2 continues its movement eastward, although the simulated system dissipates too quickly compared with the observations. On the other hand, system S1 acquires a northeastward movement and, therefore, progresses well into the Ebro valley and toward the Pyrenees (S1n). Such movement results from the generation of new convection in northern Zaragoza and northwestern Huesca along areas with strong low-level convergence: Fig. 13d exhibits a southwest–northeast convergence line across northern Zaragoza that appears to be connected with inflows into the mesolow and outflow winds arriving from S1 and S2. One hour later (Fig. 13e), the greatest convergence is found farther north, about the Zaragoza–Huesca boundary, established between the southeasterly and northwesterly flows that converge at the mesolow L1 and the new outflows from the recent convection of northern Zaragoza. As a consequence, at 1800 UTC the most important convection is affecting the northwestern quadrant of Huesca, and the connection between system S1n and the storm of Biescas (B) has already occurred (Fig. 13f). In addition, the other convective systems devel-

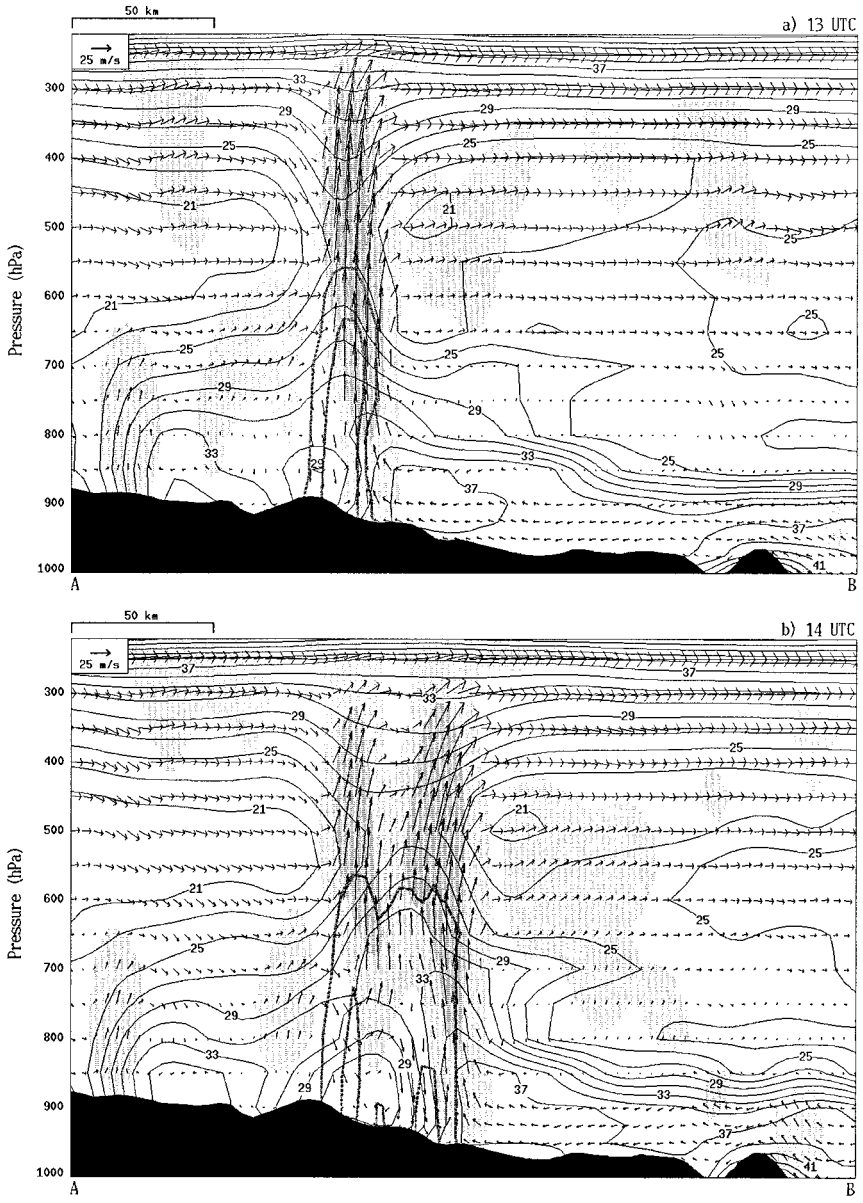

FIG. 15. Vertical cross section along the line AB depicted in Fig. 1, showing isotherms of equivalent potential temperature (continuous line, in K without the leading 3), rainwater mixing ratio contours of 0.1 and 2 g kg^{-1} (thick line), along-plane vector wind field (a reference horizontal vector is shown in the upper-left corner), and areas with vertical velocity exceeding 0.1, 2, and 5 m s^{-1} (light, medium, and dark shaded, respectively) at the following simulation times: (a) 1300, (b) 1400, (c) 1500, and (d) 1600 UTC 7 Aug 1996.

oped in southern Zaragoza and northern Teruel (S1s and S3, respectively) have grown in size and moved to the east during the 1500–1800 UTC time period. Note that we choose to identify as S1s and S3 in the simulation those convective systems that appear to be closer in space and time to the observed ones in Fig. 3 but, in fact, as the simulation time increases, a one-to-one correspondence between simulated and observed convective systems becomes impractical. It could be argued, for example, that the convective system S1s in the simulation is, instead, the one present along the border between Soria and Zaragoza in Figs. 13e–i.

It is interesting to note that the development of the convection modifies substantially the sea level pressure field, making the mesolow of the Ebro valley lose its identity with time. At 1700 UTC, for instance, the mesolow appears literally split into three distinct areas (L1, L2, and L3) by the mesohighs h1 and h2 produced by the convective systems S1n and S1s (Fig. 13e). Subsequently, with decreasing solar radiation and evapo-

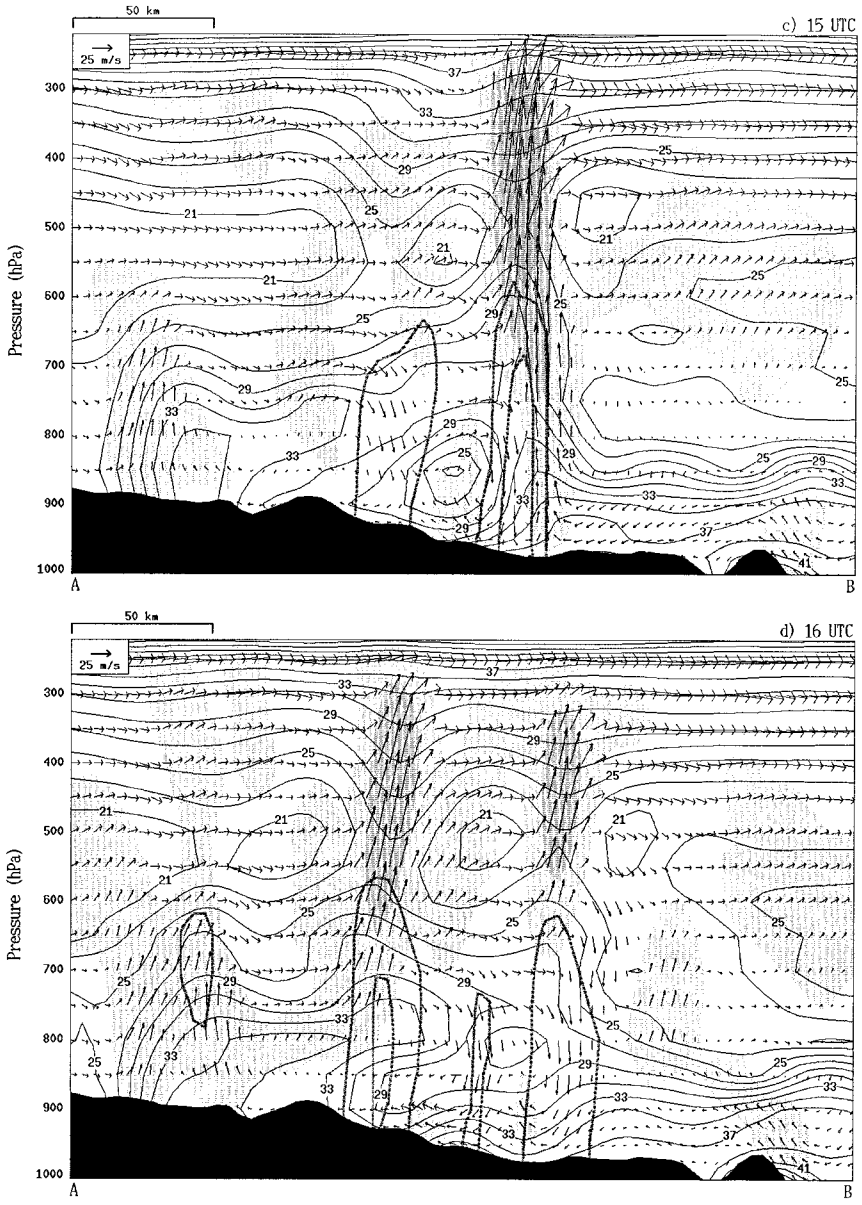

FIG. 15. (*Continued*)

ratively cooled air occupying most of the central and upper Ebro valley, the mesolow weakens and becomes much less evident. It appears that the effect of the convective cold pools becomes increasingly important during the simulation period. These cold pools tend to ''undercut'' areas of active convection, moving the convergence zones toward neighboring areas where conditionally unstable air may be lifted to its level of free convection, and so on. They appear to be responsible, therefore, for a large fraction of the movement of the convective systems through propagation (see next section).

Of particular interest is the evolution of the convection in the Biescas area (storm B). Although the rainfall rate of the simulated storm is far below the actual value (225 mm in 3 h), the simulated spatial localization and life cycle of the storm as function of time are remarkably good (cf. Figs. 3 and 13). The southward extension and gain in intensity of the storm between 1500 and 1700 UTC are captured well. The interaction of the storm with the larger system S1n approaching from the southwest after 1700 UTC, the slight extension of the merger toward the east, and its gradual dissipitation are equally correct. Such a convective sequence results from the characteristics of the low-level wind and stability in the Biescas zone and how it evolves (see next section for details). Observe that sustained southerly winds impinging against the southern slopes of the mountains are

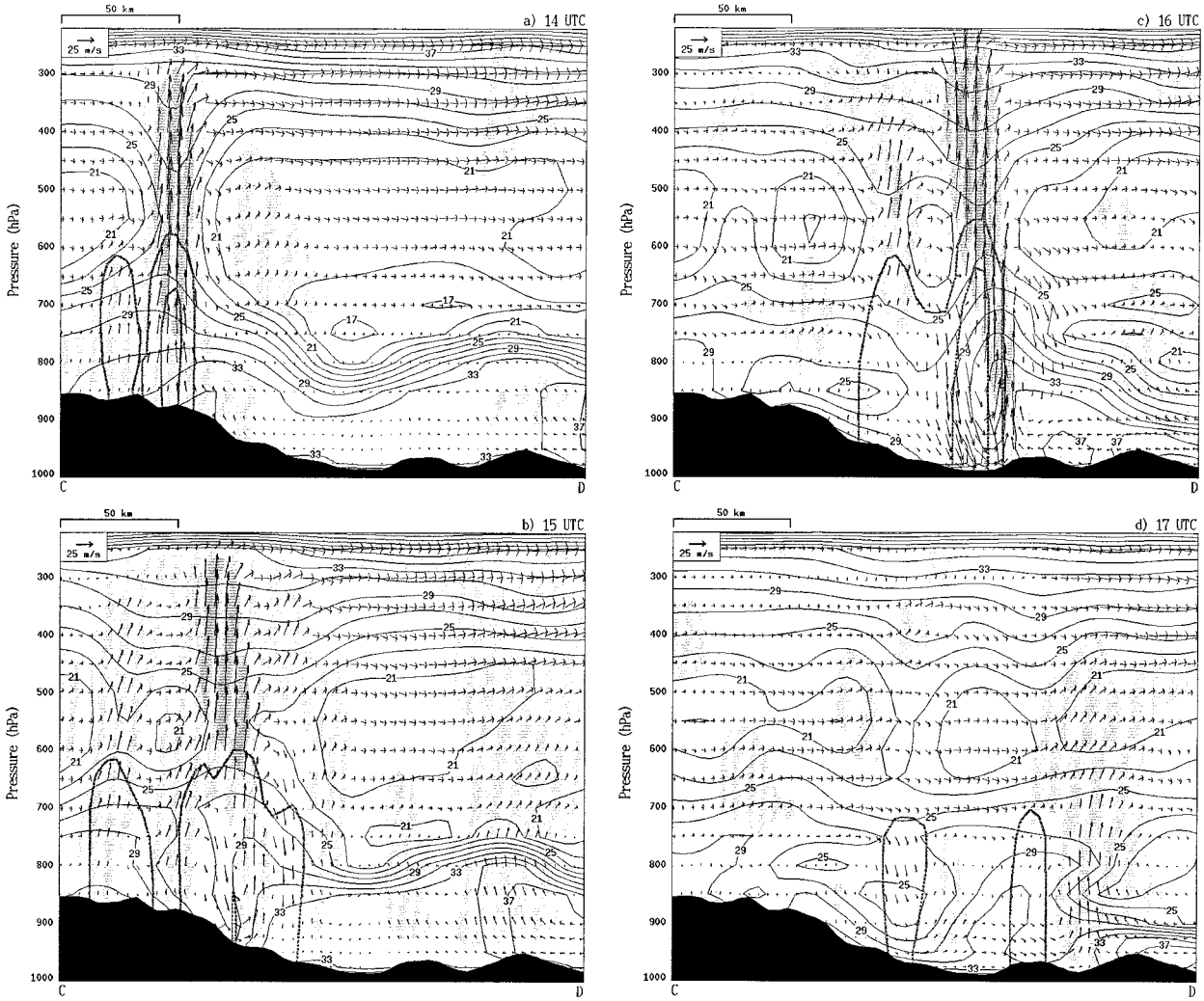

FIG. 16. As in Fig. 15 but along CD (Fig. 1) and for the following simulation times: (a) 1400, (b) 1500, (c) 1600, and (d) 1700 UTC 7 Aug 1996.

predicted until 1700 UTC (Figs. 13a–e). After the interaction with the convective system S1n, convective outflows begin to dominate in northwestern Huesca and the winds become northwesterlies, which is consistent with the analysis shown in Fig. 10b, so the low-level convergence shifts to the east and by 1900 UTC the convective mesohigh (h3) and low-level divergence are evident in the Biescas zone (Fig. 13g). Under these conditions, the system quickly dissipates (Figs. 13h and 13i).

During the last hours of 7 August, the simulated convective event departs appreciably from the observed characteristics. The simulation is able to reproduce the general dissipation of the convective cells over the Pyrenees and also the dissipation of the convective system S1s (Figs. 13g–i). The low-level winds become very weak and disorganized as a consequence of the weakening of the Ebro valley mesolow and the end of the upslope wind systems. However, the transition of the MCS S3 toward a squall line on its way to the Mediterranean (Figs. 3f–i) is not simulated. As already occurred with the previous system S2, the model is unable to develop convection in central and southern Teruel and the Mediterranean provinces. On the other hand, the model keeps developing unobserved convection to the west, in western Zaragoza, Soria, and La Rioja.

b. Vertical cross sections

Further understanding of the event can be obtained from the simulation by analyzing the vertical structure of the simulated convective systems. For such purposes, four selected vertical cross sections (indicated in Fig. 1) are presented for different times in Figs. 15–18. These cross sections reveal that a deep pool of high equivalent potential temperature (θ_e) boundary layer air advected

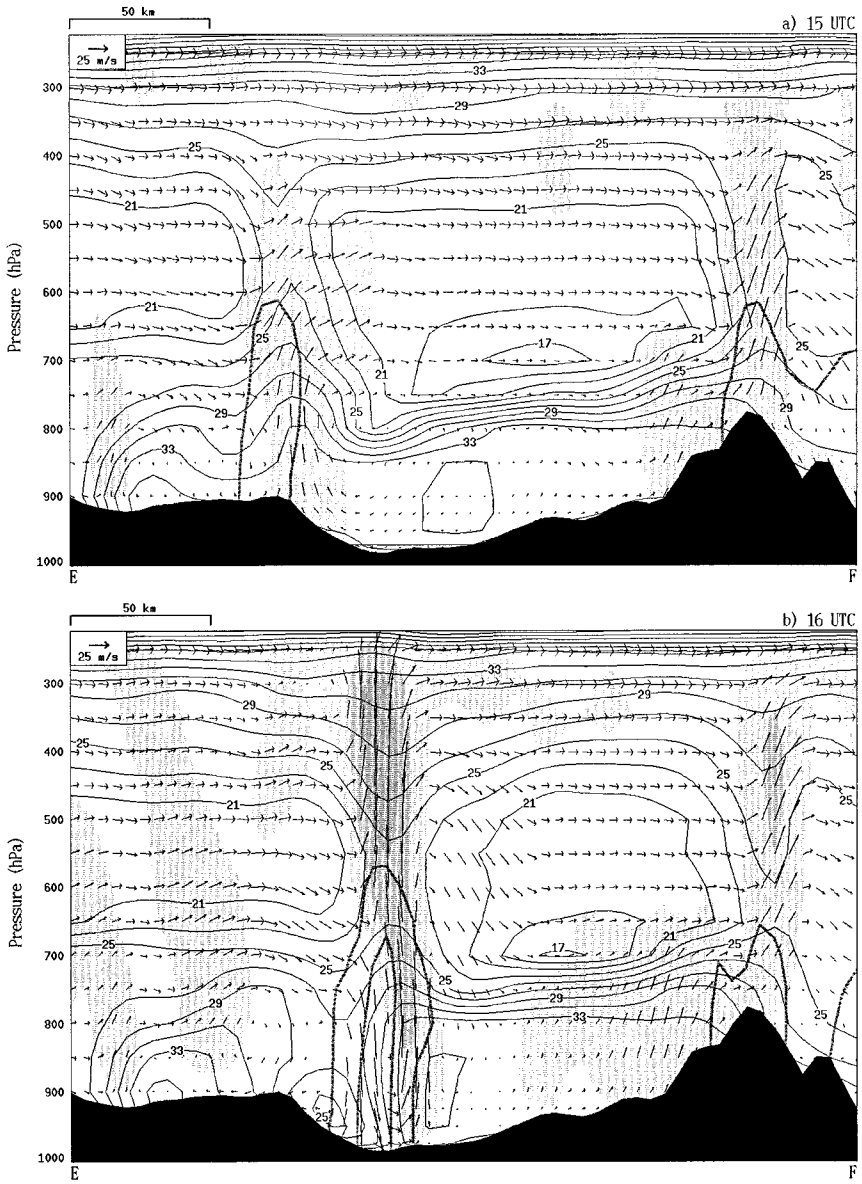

FIG. 17. As in Fig. 15 but along EF (Fig. 1) and for the following simulation times: (a) 1500, (b) 1600, (c) 1700, and (d) 1800 UTC 7 Aug 1996.

from the Mediterranean is present over the Ebro valley and adjacent slopes, contrasting with the low-θ_e air found to the southwest (left end of sections AB and EF) and north of the Pyrenees (right end of section EF). The pool of high-θ_e air is associated with marked potential instability around 800 hPa. Although the use of θ_e for the description of cold pools can, in some cases, be ambiguous because of its exponential dependence on moisture, we found a close correspondence in the lower troposphere between relative low values of θ_e and minima in the virtual potential temperature field (not shown). Under these circunstances, the use of θ_e is preferred because we are interested in describing the evolution of both the cold pools and the potential instability.

Figure 15 illustrates the convective overturning and intense cold pool generation associated with the convective system S2. While during its initial stage, the simulated system is characterized by a single deep and strong convective updraft (Fig. 15a), the spreading and intensifying low-θ_e cold pool associated with the downdraft current eventually cuts off that cell and triggers a new one to the east along the outflow boundary (Fig. 15b), where strong lifting of the high-θ_e boundary layer air is promoted. At 1500 UTC, the cold pool is very intense and the convective system has propagated farther east (Fig. 15c). However, after that time the convective cold pool appears to weaken and become elevated over the sloping terrain (Fig. 15d). The premature

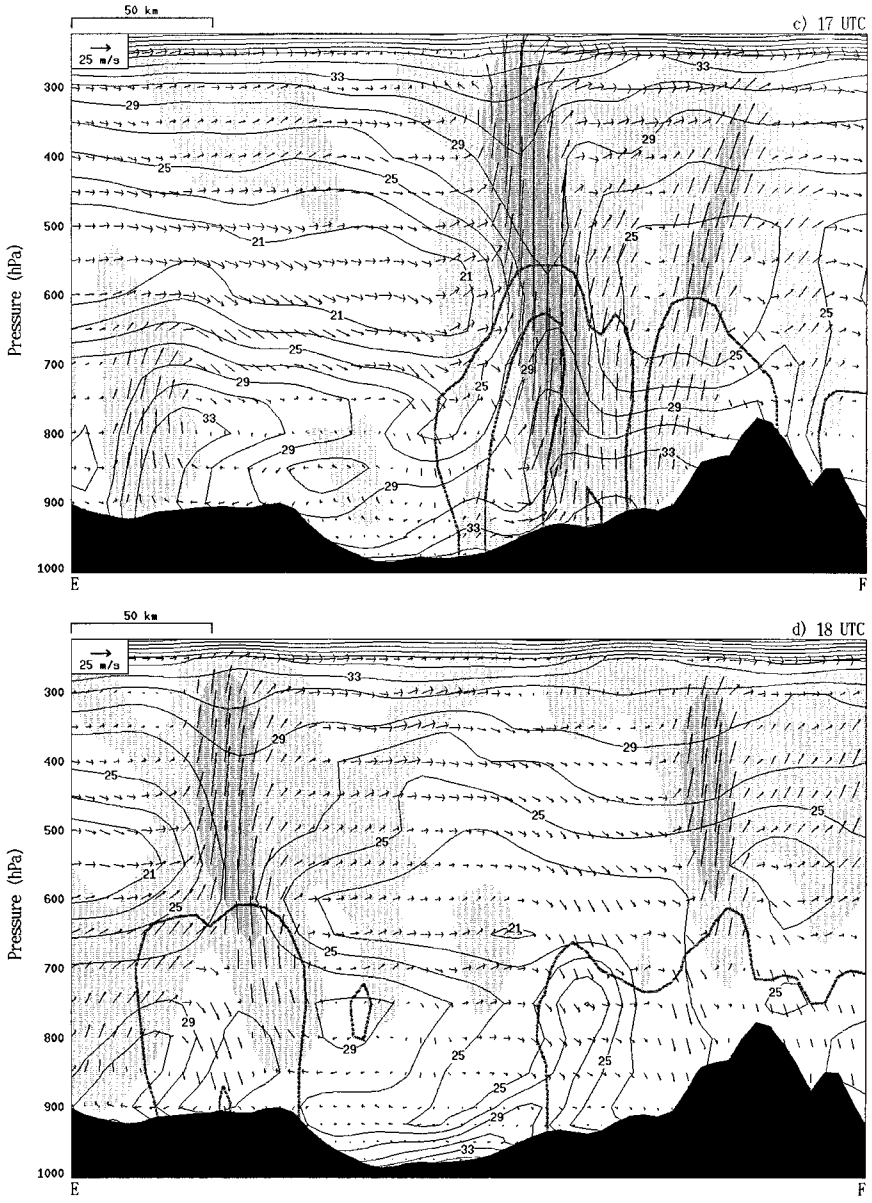

FIG. 17. (*Continued*)

dissipation of the simulated convective system S2 compared with the observations appears to be related with this loss of definition of the cold pool near the ground as it moves downslope. On the other hand, the simulated circulation of the convective system and its mode of downshear propagation, controlled by the cold pool, agree fairly well with the results of modeling studies of idealized squall lines (e.g., Rotunno et al. 1988; Weisman et al. 1988), although in the present case the flow is actually three-dimensional and the effects of the terrain and surface heating seem to be important factors.

Similarly, the incipient stage of the convective system S1 is dominated by the updraft currents (Fig. 16a). With time, the downdraft circulation and cold pool become stronger (Fig. 16b) and by 1600 UTC the multicellular character of the convective system is very clear, with a dissipating cell over the slopes of the Iberic System that has been cut off from the high-θ_e air and a new, vigorous cell that has been triggered along the outflow boundary over the plains (Fig. 16c). Later, the cold pool and outflow boundary along section CD are more poorly defined (Fig. 16d) and although significant lifting is still forced (see the plume of upward motion in the eastern part of the section), this lifting occurs now under much reduced potential instability or even stability around 800 hPa. A time sequence of the three-dimensional θ_e distribution (not included) shows that such a reduction of potential instability is motivated by the intrusion of the

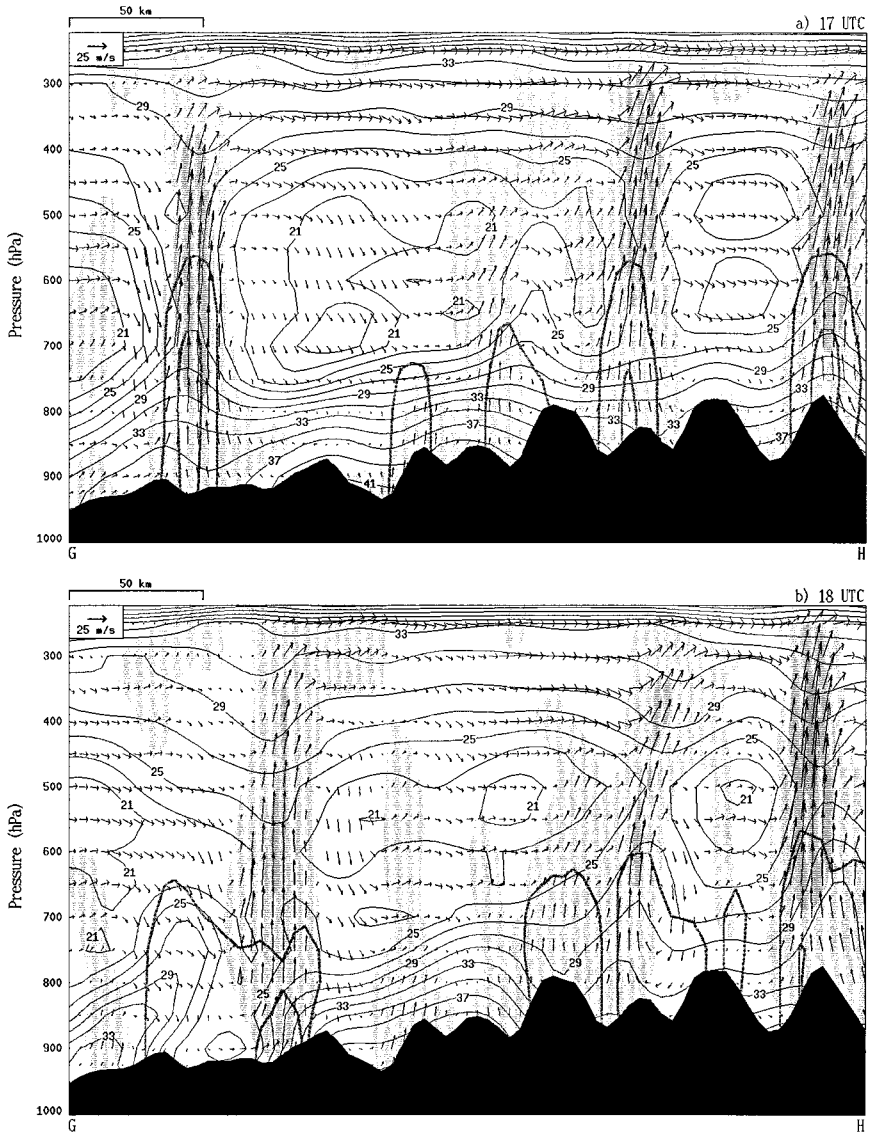

FIG. 18. As in Fig. 15 but along GH (Fig. 1) and for the following simulation times: (a) 1700, (b) 1800, (c) 1900, and (d) 2000 UTC 7 Aug 1996.

low-θ_e air seen at about 850 hPa (Fig. 16d) from the convective areas of northern Teruel. This scenario would explain the inability of the convective system S1 to propagate toward the center of the valley. Instead, new convection develops to its northeast, where lifting associated with both the convective outflow and the mesolow is intense and the stratification is potentially very unstable (Fig. 17).

The way in which this new convection (system S1n) interacts with the convection of the western Pyrenees is illustrated by the vertical cross section EF. Previous to the interaction, the simulation indicates that the convection in the Pyrenees occurs in response to the mechanical lifting of the high-θ_e boundary layer air but is restricted to the mountaintops (Fig. 17a). A plot of relative humidity (not shown) reveals that the upslope air reaches saturation near the ground and the environment is also very humid aloft, and, therefore, evaporative cooling effects are weak along the Pyrenees. Between the Pyrenees convection and the convective system S1n found to its southwest over the Iberic System slopes, convective instability is very strong but lifting processes are still weak at 1500 UTC over the bottom of the Ebro valley. In fact, the layer of strong potential instability seems to be affected by compensating subsidence associated with the upward motion that is occurrying over the slopes of the mountain ranges (Fig. 17a). However, 1 h later the lifting provided by the S1n-induced cold pool and the thermal mesolow identified in Fig. 13 is able to release the instability over the Ebro valley (Fig. 17b). Eventually, the self-propagating system S1n and the quasi-stationary con-

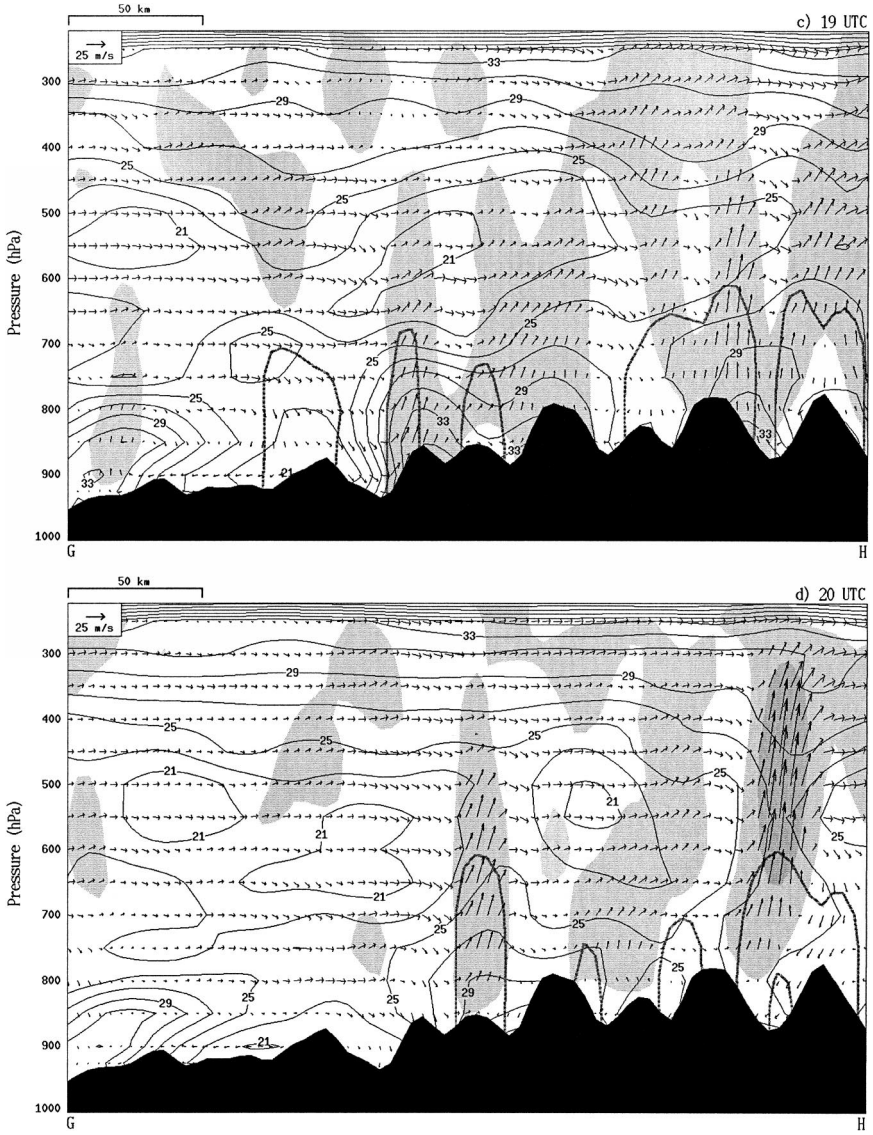

FIG. 18. (*Continued*)

vection of the Pyrenees merge together, which is seen as a very broad updraft region south of the Pyrenees peaks that is favored by the combination of the previous lifting mechanisms and the upslope flow component (Fig. 17c). However, the merging process also leads to the decay of the convection over the Pyrenees slopes because the low-θ_e downdraft air associated with the convective system S1n spreads out over the area, interrupting the upslope current of high-θ_e air. This scenario is reflected in Fig. 17d as a dissipating cell above 700 hPa over an environment of general downward motion and near-uniform values of θ_e.

The role of the S1n-induced cold pool in cutting off the supply of potentially unstable air toward the Pyrenees has been examined through the vertical cross section CH, drawn somewhat upstream of the range (Fig. 1). Indeed, the potentially unstable low-tropospheric air observed until 1700 UTC (Fig. 18a) is progressively pushed eastward by the cold pool (Figs. 18b–d). The pool of low-θ_e air is first relatively narrow (Fig. 18b), but it spreads out appreciably with time and tends to favor new updrafts along its boundaries.

c. Importance of the diurnal forcing

Both the observations and the previous simulation suggest that diurnal forcing could have been an important factor for this event. Daytime diabatic heating in the boundary layer is typically very strong over the Iberian Peninsula during summer as a consequence of the intense insolation and the very dry conditions of the semiarid terrain. The explosive character of the con-

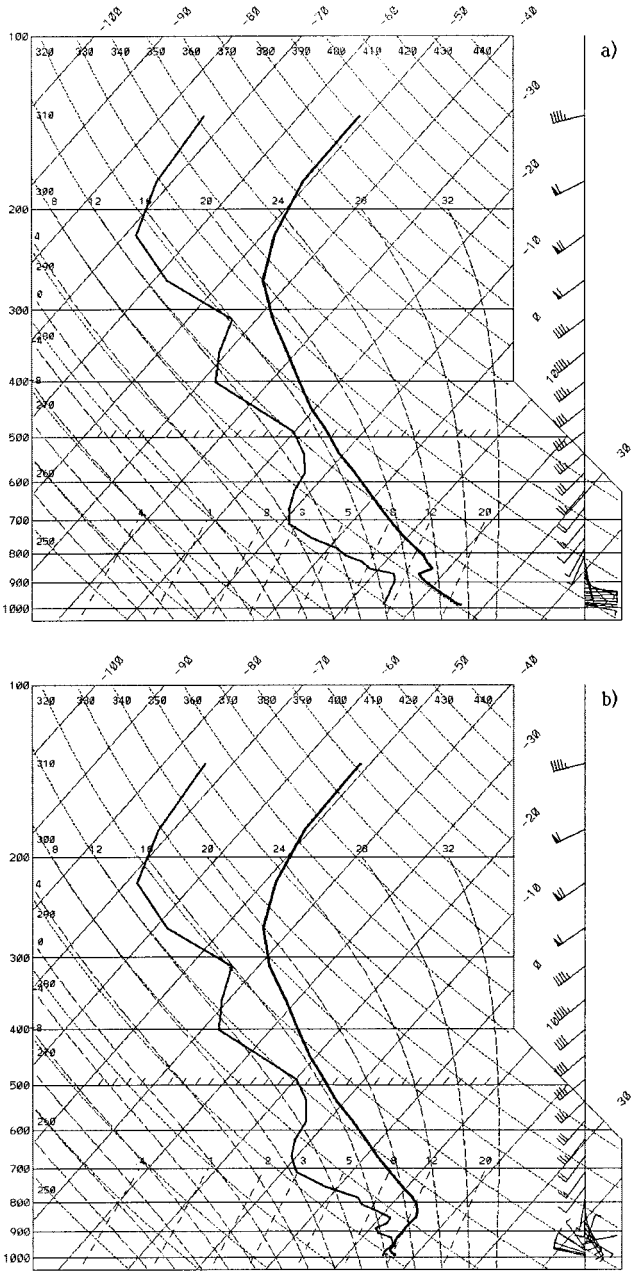

FIG. 19. Model-predicted vertical soundings at Zaragoza at 1200 UTC 7 Aug 1996 by (a) the full simulation and (b) the simulation without solar radiation. Full wind barb is 5 m s^{-1}.

vection after noon would indicate that vertical destabilization in the boundary layer was necessary for the outbreak of the convection. Moreover, determinant features of the low-level flow, such as the mesolow in the Ebro valley and the sustained upslope winds, appear to be linked to the diurnal cycle. Therefore, it is worthwhile to investigate explicitly the role of the diurnal forcing for this case study. With this aim, another numerical simulation was performed, identical to the previous one, but excluding solar radiation from the model physics.

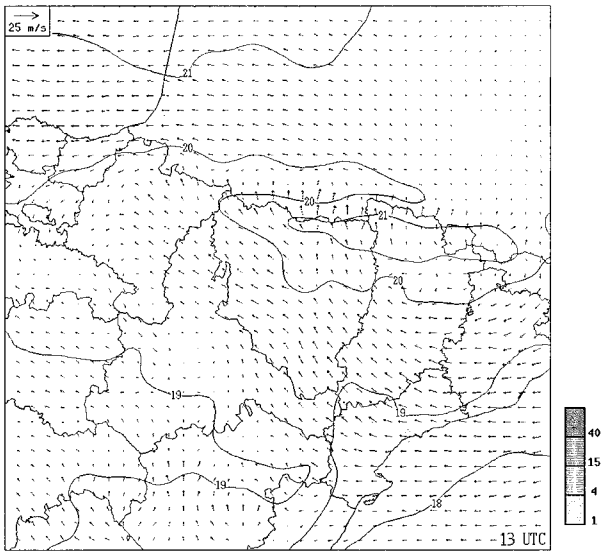

FIG. 20. As in Fig. 13 except for the simulation without solar radiation and at 1300 UTC 7 Aug.

Obviously, the importance of insolation for the boundary layer destabilization is well known. A selected model sounding from the city of Zaragoza (Fig. 19) is quite illustrative. A convective, well-mixed boundary layer develops in the full simulation (Fig. 19a), whereas the boundary layer is much cooler and more stable without solar radiation (Fig. 19b), resulting in much larger amounts of CIN for the near-surface parcels to overcome.

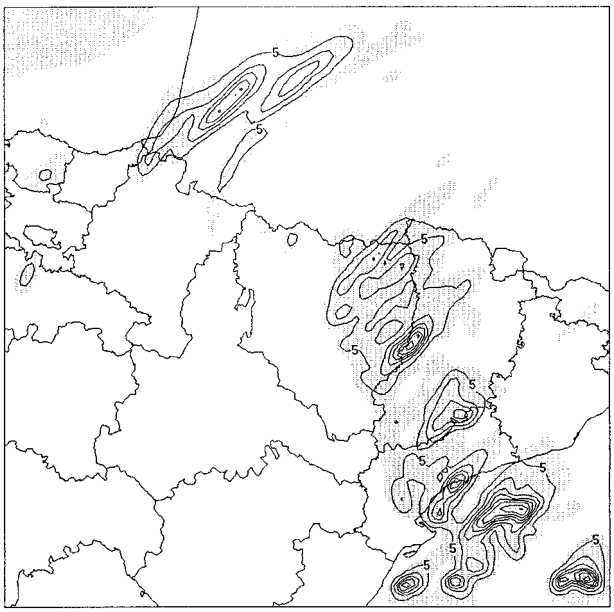

FIG. 21. As in Fig. 12 except for the simulation without solar radiation.

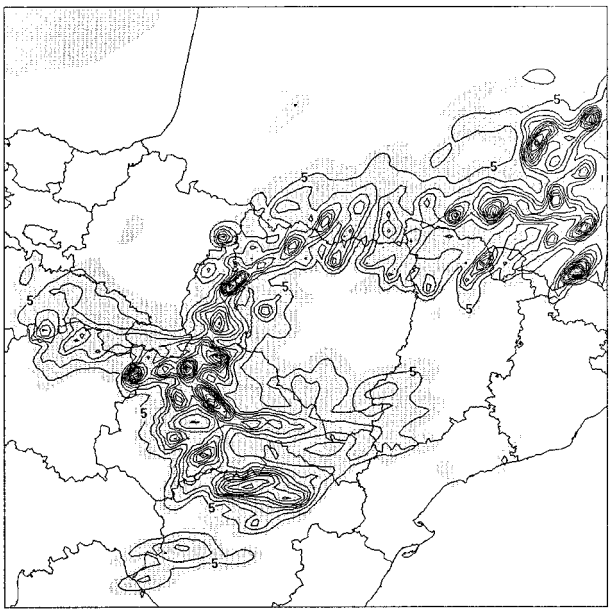

FIG. 22. As in Fig. 12 except for the simulation without evaporative cooling.

The simulated Zaragoza sounding shown in Fig. 19a can be compared with the observed one (Fig. 7b). The temperature and wind profiles above the boundary layer appear to be very well simulated. In contrast, the heating in the boundary layer is stronger and the position of the inversion lower than indicated by the observations. The simulated environment is also generally drier than observed. Other model soundings from adjacent locations that were affected, unlike central Zaragoza, by significant convection during the afternoon (northern Teruel, western and northern Zaragoza; not shown) exhibit thermodynamic structures very similar to the previous one. Therefore, the spatial distribution of the convective activity is clearly linked to the spatial localization of the lifting mechanisms identified in the previous sections, not to a coexistence of significantly different thermodynamic environments.

The strong diurnal dependence of the low-level flow can be appreciated by comparing the results of the present simulation (Fig. 20) and the full simulation (Fig. 13a). It can be observed that without diurnal heating, the pressure gradient is much weaker and the mesolow of the Ebro valley does not develop. This supports the hypothesis that the mesolow has a thermal origin. Further, the widespread upslope wind systems obtained in the full simulation are less pronounced or absent in this case; the winds are generally weaker and more parallel to the Pyrenees and Iberic ranges.

As expected, without the diurnal effects, the convection develops later and farther east, along a broad band extending between northeastern Huesca and the Mediterranean waters (Fig. 21). Presumably, most of the warm season convection that regularly affects northeastern Spain depends critically on diurnally forced features of the flow for its initiation and spatial localization.

d. Importance of the cold pools and associated outflows

The full simulation presented in sections 4a and 4b also indicated that evaporatively induced cold pools and their associated outflows, continuously emerging from areas of convection, eventually become a dominant aspect of the flow and are largely responsible for the propagation of the convective systems. In order to investigate these actions, another simulation was designed in which the cooling due to evaporation of rain falling through subsaturated layers was not incorporated in the model temperature tendency equation.

The forecast total precipitation by this simulation is displayed in Fig. 22, which should be compared with the results of the full run (Fig. 12) and the observed rainfall (Fig. 2a). As can be observed, the general spatial pattern of the precipitation field remains basically unchanged. However, the precipitation is substantially lower than observed around the Soria–Guadalajara–Zaragoza triple point, too excessive in eastern Zaragoza and northern Teruel, and most notably, an unrealistic broad area of too much rainfall crossing Zaragoza from south to north is simulated. These structures result from an incorrect timing of the event and lack of propagation of the convection, which remains almost stationary over the province of Zaragoza. The reader can compare the predicted hourly rainfall from the full simulation (Fig. 13) with that resulting from the evaporative cooling free experiment (Fig. 23). The latter is shown only from 1500 UTC, since the results from the previous 2 h are similar to the full run, meaning that the initial outflows from the first convection were not very important during the beginning of the event.

The importance of the cold pools for the organization of the low-level flow is already evident at 1500 UTC. For instance, with no cold pool, the winds in south-central Zaragoza are from the east (Fig. 23a) instead of southeasterlies (Fig. 13c), and the mesolow appears more elongated along the Ebro valley contrary to what the analysis of Fig. 9a suggests. After 1600 UTC, the simulation without cold pools starts to depart appreciably from the full run and the available observations. Note, for instance, that the observed sea level pressure distribution at 1800 UTC (Fig. 10a), in the form of a relative high pressure area toward southern Zaragoza and Teruel flanked by relative low pressures to its northeast and northwest, is in this case not simulated at all. The entrance of the northwesterly flow in western Huesca (Fig. 10b) is not simulated either. Figures 23b–g indicate that in the no-evaporation run continuous and almost stationary convective developments occur over the province of Zaragoza in response to the low-level convergence induced by the thermal mesolow of the Ebro valley. This mesolow tends to migrate toward the

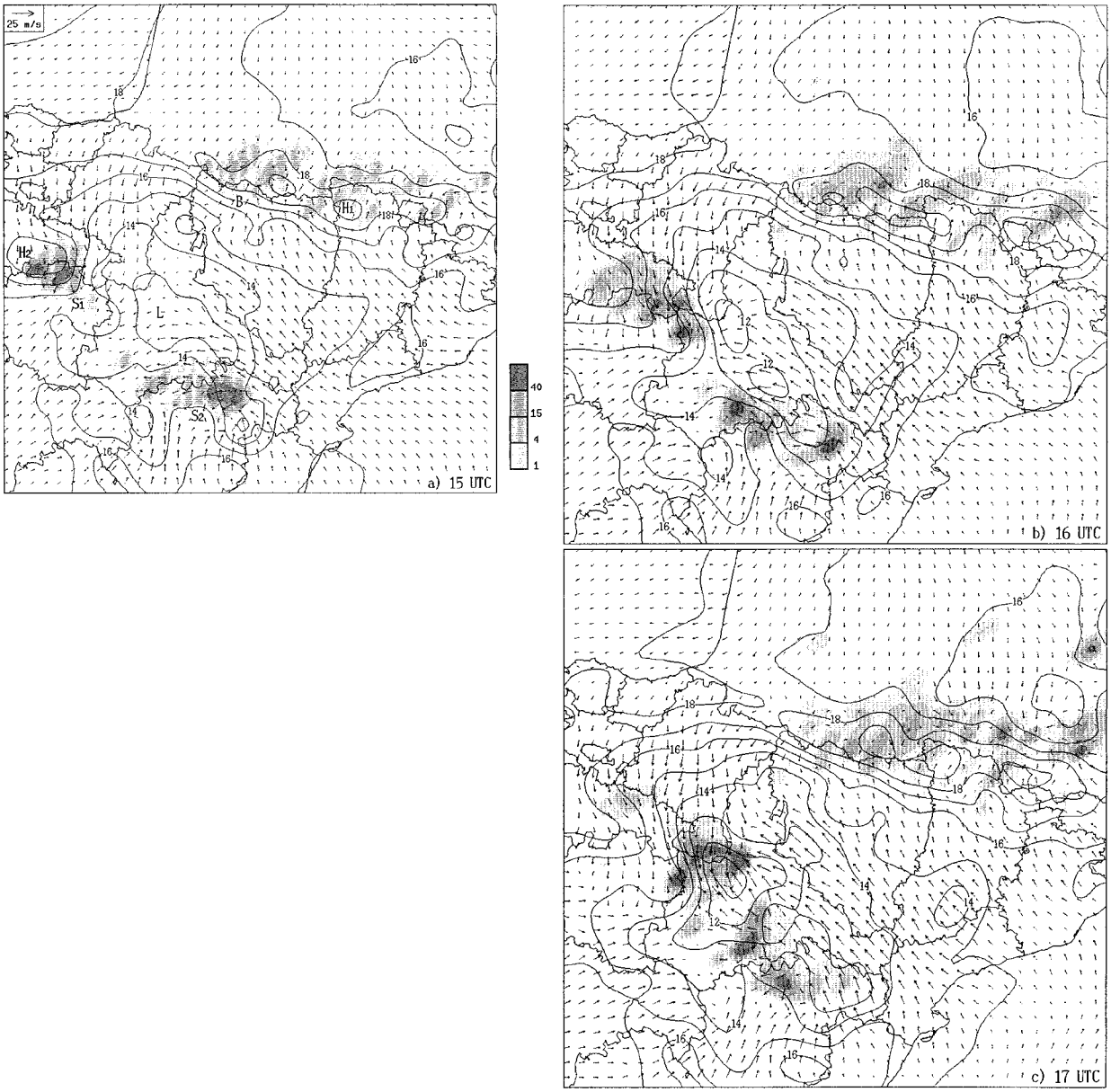

FIG. 23. As in Fig. 13, except for the simulation without evaporative cooling and for the period 1500–2100 UTC 7 Aug 1996.

lower part of the valley with time, but in contrast with the full run (recall Fig. 13), it is deeper and keeps its structure and intensity. Without the evolving cold pools continuously disturbing the pressure pattern, the wind field eventually defines a quite strong cyclonic circulation over the Ebro valley (Fig. 23g). Interestingly, the connection between the MCS of Zaragoza and the storm of Biescas is still produced, but after that, the resulting convective line remains intense and quasistationary till its dissipation at 2100 UTC.

It seems, therefore, that the convectively generated cold pools and outflows were indeed very important for the evolution of the simulated convection. The cold pools naturally acted to stabilize the environment, and the accompanying outflows helped to propagate the convection quite in the same way as indicated by the observations, avoiding unrealistic, excessive precipitation in the areas dominated by the mesolow. Of course, these actions are particular to this case study and may not be generalizable. There can be many other cases where the convective outflows can have the opposite effect: to favor quasistationary convective systems instead of mobile ones.

5. Concluding remarks

Our case study has shown the importance of mesoscale components of the flow for the initiation, move-

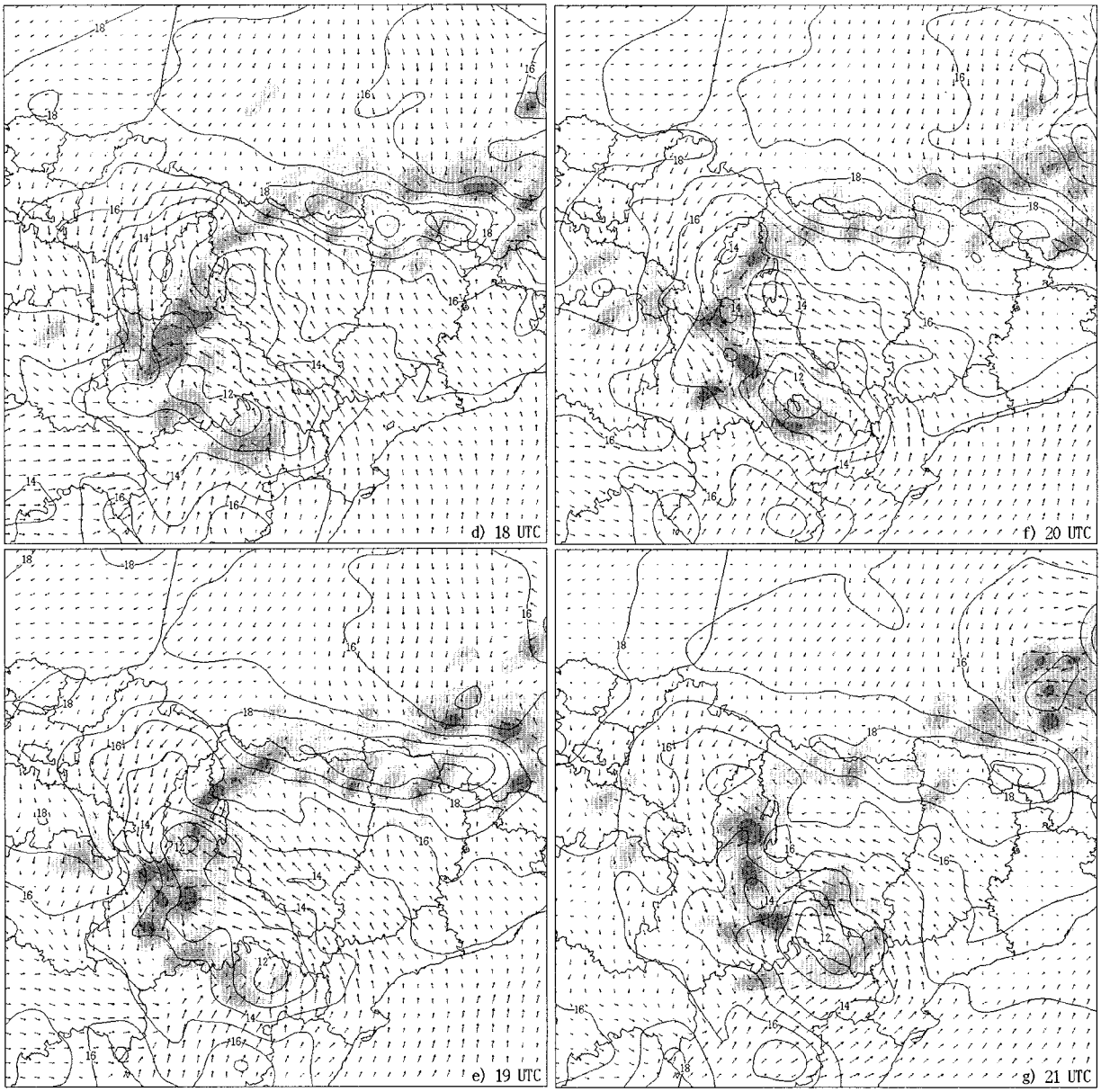

FIG. 23. (*Continued*)

ment, and life cycle of convection. Outside of environments characterized by strong and well-defined large-scale forcing for upward motion, it is logical to propose that many convective events are strongly modulated by mesoscale processes (Stensrud and Fritsch 1993). Therefore, succesful application of numerical models for detailed forecasts of convection certainly demands the ability of the system to capture fine spatial and temporal features of the flow, either by their explicit prediction or by assimilating them during the initialization or forecast period. Of course, this requirement poses a practical limit to the attainable predictability of convection, owing to the limited resolution of standard observations, although efforts directed to ingest mesonet data and the quasi-continuous radar and satellite information into numerical models are certainly promising (Wilson et al. 1998).

For our case study in northeastern Spain, a simulation using a moderately fine horizontal grid resolution (4 km) but a conventional initialization is able to provide reasonably accurate information of the convective event that would have been of value to forecasters. The simulated timing of the convection is especially remarkable, although such timing accuracy may not always be possible. In this particular case, the strong orographic influences typical of the region and the leading role of diurnally forced circulations (mesolow in the Ebro valley and upslope winds) seem to favor the predictability

of the event, since both processes tend to be well handled by the mesoscale model. This suggests that model grid resolution and physical parameterizations are quite important. However, the simulated convective outbreak also has illustrated clearly the important role of convectively induced features embedded in the flow for the control of the convection itself, notably its propagation mode. The simulation performed without active cold pools produced a degraded forecast in spite of the correct prediction of the other nonconvective mesoscale features and the correct location and timing of the first convection.

Despite the well-recognized importance of convective cold pools and associated outflows, these elements are often not well sampled by the present observational network and are rarely depicted in mesoscale model initial conditions. Undoubtedly, the production of more realistic model initial conditions may be beneficial for heavy precipitation forecasting. A procedure devised by Stensrud et al. (1999) to identify and insert cold pools into a mesoscale model was shown to improve the numerical guidance for weakly forced synoptic situations. Further, although cold pools might not be present at the initial time, the model has to be able to develop these pools adequately. This is feasible in a research context if the grid resolution allows an explicit modeling of convection and complex microphysical schemes are used (Davis and Weisman 1999), as for example in our case study. However, some convective parameterization schemes currently used in the operational context are unable to develop or assist in the maintenance of cold pools owing to the lack of a downdraft parameterization [e.g., the Betts–Miller scheme; Betts (1986); Betts and Miller (1986)]. Other convective parameterization schemes incorporate convective downdrafts [e.g., the Kain–Fritsch scheme; Kain and Fritsch (1990)] but their treatment is not always very realistic. Spencer and Stensrud (1998) showed that if an updraft–downdraft time lag as suggested by observations was allowed in the Kain–Fritsch scheme, simulations of several flash flood events generally outperformed the results using the default scheme, in which updrafts and downdrafts are assumed to occur simultaneously. Clearly, improved parameterizations of convective downdrafts will increase the potential of mesoscale numerical models for heavy precipitation forecasting.

Acknowledgments. We gratefully acknowledge constructive comments on an earlier version of this manuscript from Dr. David Stensrud, Dr. Conrad Ziegler, and two anonymous reviewers. This work was partially developed while the first author held a National Research Council–National Severe Storms Laboratory Research Associateship, and completed under support of the Scientific Program of NATO. Also, computer support provided by NCAR's Scientific Computer Division (which is sponsored by the National Science Foundation) for model data preprocessing is acknowledged. Observational data of the event was provided by the Spanish Instituto Nacional de Meteorología.

REFERENCES

Alonso, S., A. Portela, and C. Ramis, 1994: First considerations on the structure and development of the Iberian thermal low. *Ann. Geophys.,* **12,** 457–468.

Benjamin, S. G., 1983: Some effects of heating and topography on the regional severe storm environment. Ph.D. thesis, The Pennsylvania State University, 265 pp.

——, and N. L. Seaman, 1985: A simple scheme for improved objective analysis in curved flow. *Mon. Wea. Rev.,* **113,** 1184–1198.

Betts, A. K., 1986: A new convective adjustment scheme. Part I: Observational and theoretical basis. *Quart. J. Roy. Meteor. Soc.,* **112,** 677–692.

——, and M. J. Miller, 1986: A new convective adjustment scheme. Part II: Single column tests using GATE wave, BOMEX, ATEX and Arctic air-mass data sets. *Quart. J. Roy. Meteor. Soc.,* **112,** 693–709.

Blackadar, A. K., 1979: High resolution models of the planetary boundary layer. *Advances in Environmental Science and Engineering,* J. Pfafflin and E. Ziegler, Eds., Vol. 1, No. 1, Gordon and Breach, 50–85.

Brooks, H. E., and C. A. Doswell III, 1993: New technology and numerical weather prediction: A wasted opportunity? *Weather,* **48,** 173–177.

——, M. S. Tracton, D. J. Stensrud, G. DiMego, and Z. Toth, 1995: Short-range ensemble forecasting: Report from a workshop (25–27 July 1994). *Bull. Amer. Meteor. Soc.,* **76,** 1617–1624.

Chappell, C. F., 1986: Quasi-stationary convective events. *Mesoscale Meteorology and Forecasting,* P. S. Ray, Ed., Amer. Meteor. Soc., 289–310.

Colle, B. A., and C. F. Mass, 1996: An observational and modeling study of the interaction of low-level southwesterly flow with the Olympic Mountains during COAST IOP4. *Mon. Wea. Rev.,* **124,** 2152–2175.

Davis, C. A., and M. L. Weisman, 1999: MM5 as a cloud model. Preprints, *Ninth PSU/NCAR Mesoscale Model Users' Workshop,* Boulder, CO, NCAR, 168–171.

Doswell, C. A., III, 1987: The distinction between large-scale and mesoscale contribution to severe convection: A case study example. *Wea. Forecasting,* **2,** 3–16.

Dudhia, J., 1989: Numerical study of convection observed during the Winter Monsoon Experiment using a mesoscale two-dimensional model. *J. Atmos. Sci.,* **46,** 3077–3107.

——, 1993: A nonhydrostatic version of the Penn State/NCAR mesoscale model: Validation tests and simulation of an Atlantic cyclone and cold front. *Mon. Wea. Rev.,* **121,** 1493–1513.

Grell, G. A., 1993: Prognostic evaluation of assumptions used by cumulus parameterizations. *Mon. Wea. Rev.,* **121,** 764–787.

——, J. Dudhia, and D. R. Stauffer, 1995: A description of the fifth-generation Penn State/NCAR mesoscale model (MM5). NCAR Tech. Note NCAR/TN-398+STR, 122 pp.

Hoskins, B. J., and M. A. Pedder, 1980: The diagnosis of middle latitude synoptic development. *Quart. J. Roy. Meteor. Soc.,* **106,** 707–719.

Kain, J. S., and J. M. Fritsch, 1990: A one-dimensional entraining/detraining plume model and its application in convective parameterization. *J. Atmos. Sci.,* **47,** 2784–2802.

Koistinen, J., and T. Puhakka, 1984: Can we calibrate radar by raingauges. Preprints, *22d Conf. on Radar Meteorology,* Zurich, Switzerland, Amer. Meteor. Soc., 263–267.

Lin, Y. L., R. D. Farley, and H. D. Orville, 1983: Bulk parameterization of the snow field in a cloud model. *J. Climate Appl. Meteor.,* **22,** 1065–1092.

Mass, C. F., and Y. H. Kuo, 1998: Regional real-time numerical weath-

er prediction: Current status and future potential. *Bull. Amer. Meteor. Soc.,* **79,** 253–263.

Riosalido, R., and Coauthors, 1998: Estudio meteorológico de la situación del 7 de Agosto de 1996 (Biescas). Nota Técnica STAP 26, 90 pp. [Available from Instituto Nacional de Meteorología, Apartado 285, 28071 Madrid, Spain.]

Romero, R., C. A. Doswell III, and C. Ramis, 2000: Mesoscale numerical study of two cases of long-lived quasistationary convective systems over eastern Spain. *Mon. Wea. Rev.,* **128,** 3731–3751.

Rotunno, R., J. B. Klemp, and M. L. Weisman, 1988: A theory for strong, long-lived squall lines. *J. Atmos. Sci.,* **45,** 463–485.

Spencer, P. L., and D. J. Stensrud, 1998: Simulating flash flood events: Importance of the subgrid representation of convection. *Mon. Wea. Rev.,* **126,** 2884–2912.

Stensrud, D. J., and J. M. Fritsch, 1993: Mesoscale convective systems in weakly forced large-scale environments. Part I: Observations. *Mon. Wea. Rev.,* **121,** 3326–3344.

——, and ——, 1994: Mesoscale convective systems in weakly forced large-scale environments. Part II: Generation of a mesoscale initial condition. *Mon. Wea. Rev.,* **122,** 2068–2083.

——, G. S. Manikin, E. Rogers, and K. E. Mitchell, 1999: Importance of cold pools to NCEP mesoscale Eta Model forecasts. *Wea. Forecasting,* **14,** 650–670.

Tao, W. K., and J. Simpson, 1993: Goddard cumulus ensemble model. Part I: Model description. *Terr. Atmos. Oceanic Sci.,* **4,** 35–72.

Washington, W. M., and D. P. Baumhefner, 1975: A method of removing Lamb waves from initial data for primitive equation models. *J. Appl. Meteor.,* **14,** 114–119.

Weisman, M. L., J. B. Klemp, and R. Rotunno, 1988: The structure and evolution of numerically simulated squall lines. *J. Atmos. Sci.,* **45,** 1990–2013.

——, W. C. Skamarock, and J. B. Klemp, 1997: The resolution dependence of explicitly modeled convective systems. *Mon. Wea. Rev.,* **125,** 527–548.

Wilson, J. W., N. A. Crook, C. K. Mueller, J. Sun, and M. Dixon, 1998: Nowcasting thunderstorms: A status report. *Bull. Amer. Meteor. Soc.,* **79,** 2079–2100.

Zhang, D. L., 1989: The effect of parameterized ice microphysics on the simulation of vortex circulation with a mesoscale hydrostatic model. *Tellus,* **41A,** 132–147.

——, and R. A. Anthes, 1982: A high-resolution model of the planetary boundary layer—Sensitivity tests and comparisons with SESAME-79 data. *J. Appl. Meteor.,* **21,** 1594–1609.

——, and J. M. Fritsch, 1986: Numerical simulation of the meso-β scale structure and evolution of the 1977 Johnstown flood. Part I: Model description and verification. *J. Atmos. Sci.,* **43,** 1913–1943.

——, H. R. Chang, N. L. Seaman, T. T. Warner, and J. M. Fritsch, 1986: A two-way interactive nesting procedure with variable terrain resolution. *Mon. Wea. Rev.,* **114,** 1330–1339.

——, K. Gao, and D. B. Parsons, 1989: Numerical simulation of an intense squall line during 10–11 June 1985 PRE-STORM. Part I: Model verification. *Mon. Wea. Rev.,* **117,** 960–994.